

# Stabilizing discrete empirical interpolation via randomized and deterministic oversampling

Benjamin Peherstorfer\*    Zlatko Drmač†    Serkan Gugercin‡

November 9, 2018

This work investigates randomized and deterministic oversampling in (discrete) empirical interpolation for nonlinear model reduction. Empirical interpolation derives approximations of nonlinear terms from a few samples via interpolation in low-dimensional spaces. It has been demonstrated that empirical interpolation can become unstable if the samples from the nonlinear terms are perturbed due to, e.g., noise, turbulence, and numerical inaccuracies. We demonstrate with a probabilistic analysis that randomized oversampling stabilizes empirical interpolation in the presence of noise. Furthermore, we discuss deterministic oversampling strategies that select points by descending in directions of eigenvectors corresponding to sampling point updates and by establishing connections between sampling point selection and clustering. Numerical experiments with synthetic and diffusion-reaction problems demonstrate the stability of oversampled empirical interpolation in the presence of noise.

**Keywords:** model reduction; empirical interpolation, sparse sampling, oversampling, noisy observations, randomized model reduction, probabilistic analysis, proper orthogonal decomposition, nonlinear model reduction

## 1 Introduction

Model reduction seeks to construct reduced systems that provide accurate approximations of the solutions of large-scale systems of equations with significantly reduced computational cost [9]. In projection-based model reduction, the reduced systems are obtained via (Petrov-)Galerkin projection of the full-system equations onto low-dimensional—reduced—subspaces of the high-dimensional solution spaces corresponding to the full systems. If the large-scale systems contain nonlinear equations, then projection of the full-system equations onto reduced spaces typically is insufficient to obtain reduced systems that are computationally cheaper to solve than the full systems, because the nonlinear terms entail computations with costs that scale with the number of the degrees of freedom of the full system. Empirical interpolation [7,31,32], and its discrete counterpart, the discrete empirical interpolation method (DEIM) [17,22], provide one solution to this problem by approximating the nonlinear terms of the nonlinear equations via sparse sampling. The nonlinear terms are evaluated at a few interpolation points—sampling points—and then all other components of the nonlinear

---

\*Courant Institute of Mathematical Sciences, New York University, New York, NY 10012. The work of Peherstorfer is supported in parts by the Air Force Center of Excellence on Multi-Fidelity Modeling of Rocket Combustor Dynamics, Award Number FA9550-17-1-0195.

†Faculty of Science, Department of Mathematics, University of Zagreb, Bijenička 30, 10000 Zagreb, Croatia. The work of Drmač is supported in parts by the Croatian Science Foundation through Grant HRZZ-9345.

‡Department of Mathematics, Virginia Polytechnic Institute and State University, 460 McBryde, Virginia Tech, Blacksburg, VA 24061-0123. The work of Gugercin is supported in parts by NSF through Grant DMS-1522616.

terms are approximated via interpolation in low-dimensional subspaces. However, approximations via (D)EIM have been shown to suffer from instabilities in certain situations, see, e.g., [2, 26, 48]. Localization [24, 37] and adaptation [38] of the low-dimensional subspaces have been proposed as possible remedies. Another remedy that has been reported in the literature, and that typically is easier to implement in practice than localization and adaptation, is oversampling empirical interpolation so that the nonlinear terms are approximated via regression rather than via interpolation [2, 4, 14, 48, 50]. In this work, we consider the specific case where only noisy samples—observations—of the nonlinear terms are available and where DEIM has been shown to be unstable, see, e.g., [2]. We provide a probabilistic analysis that shows that oversampling DEIM leads to stable approximations even in the presence of noisy samples and propose deterministic oversampling strategies to select oversampling points in principled ways.

Oversampling in empirical interpolation has been investigated. Missing point estimation (MPE) [3, 4] relies on gappy proper orthogonal decomposition (POD) [25] to approximate nonlinear terms in model reduction and derives approximations via regression, instead of interpolation. Several sampling point selection algorithms have been proposed for MPE and gappy POD. The work [46] formulates point selection as a sensor placement problem and proposes a greedy approach to find an approximate solution. Detailed analyses of point selection for MPE, and screening approaches to speedup point selection, are provided in [4]. The work by Zimmermann et al. [50] introduces a sampling strategy for MPE that is based on approximating eigenvalues for selecting sampling points and demonstrates that oversampling achieves higher accuracies in numerical experiments in computational fluid dynamics than MPE without oversampling. We will arrive at a special case of the approach presented in [50] via perturbation bounds on eigenvalues introduced in [30]. Carlberg et al. [15, 16] introduce the Gauss-Newton with approximated tensors (GNAT) method that is based on Petrov-Galerkin projection and approximates the nonlinear terms via low-cost least-squares problems. The GNAT method and its performance based on regression has been investigated in the thesis [14], where a greedy-based deterministic sampling strategy for selecting oversampling points has been proposed. Zhou [48] introduces a deterministic oversampling strategy for DEIM that exploits the dependency of the degrees of freedom of the full system to select oversampling points. Oversampling is then applied to multi-scale problems, where DEIM with Zhou’s oversampling achieves lower errors than DEIM without oversampling. The adaptive DEIM (ADEIM), which adapts the DEIM space from sparse samples of the nonlinear terms, is based on regression [38, 49], even though regression is used for adaptation only and the nonlinear terms are approximated via interpolation once the DEIM interpolants have been adapted. Oversampling strategies for DEIM are investigated by Kutz et al. [33], who showed improvements if DEIM is used for signal reconstruction [34, 41]. Greedy methods for sensor placement in the context of empirical interpolation are investigated in [1, 10].

We consider oversampling of DEIM in the specific setting where evaluations of the nonlinear terms are polluted with noise. Noise is here to be understood in general terms, including perturbations that are typically modeled via random noise such as in turbulence, see, e.g., [40]. It has been discussed in [2] that the  $L_2$  error of DEIM approximations can grow with the dimension of the DEIM space in presence of noise. The work [2] proposes oversampling as a possible remedy and demonstrates on numerical results that oversampling stabilizes DEIM, i.e., that the error of the oversampled DEIM does not increase with the DEIM dimension. We build on the vast oversampling literature [3, 4, 15, 16, 33, 48, 50]. Our contribution is a probabilistic analysis that proves that in expectation with high probability oversampling avoids the increase of the  $L_2$  error with the dimension of the DEIM space. For the analysis, we follow the work by Balzano et al. [6] and the work by Cohen et al. [20] that provide approximation results for least-squares approximations, which we apply to oversampled DEIM. Extensions to the work by Cohen et al. [20] have been introduced in [19, 35]. We then discuss two deterministic oversampling strategies and demonstrate with numerical results that a lower error with oversampling and regression is achieved compared to classical DEIM that interpolates the nonlinear terms.

The structure of the paper is as follows. Section 2 briefly reviews DEIM in the context of model reduction and numerically demonstrates on a toy example that DEIM approximations are unstable if the nonlinear function evaluations are polluted with noise. Section 3 and Section 4 analyze oversampling DEIM and prove

that oversampling avoids the stability issue in expectation with high probability. Section 5 introduces two deterministic oversampling strategies, which are then shown to achieve more accurate reduced models than classical DEIM in Section 6.

## 2 Preliminaries and problem formulation

This section briefly reviews DEIM for approximating the nonlinear terms in reduced models and demonstrates, via an example, that DEIM can become unstable in the case of noisy evaluations of these nonlinear terms.

### 2.1 Model reduction with discrete empirical interpolation

Consider a system of parametrized nonlinear equations

$$\mathbf{A}\mathbf{x}(\boldsymbol{\xi}) + \mathbf{f}(\mathbf{x}(\boldsymbol{\xi}); \boldsymbol{\xi}) = 0, \quad (1)$$

where  $\mathbf{x}(\boldsymbol{\xi}) \in \mathbb{R}^N$  is the state,  $\boldsymbol{\xi} \in \mathcal{D}$  is a  $d$ -dimensional parameter in the parameter domain  $\mathcal{D}$ ,  $\mathbf{A} \in \mathbb{R}^{N \times N}$  is a constant matrix, and  $\mathbf{f} : \mathbb{R}^N \times \mathcal{D} \rightarrow \mathbb{R}^N$  is a nonlinear function. Systems such as eq. (1) typically arise after discretizing a PDE in the spatial domain, in which case the matrix  $\mathbf{A}$  corresponds to the linear operators in the underlying PDE and the nonlinear function  $\mathbf{f}$  to the nonlinear terms. In the following, we are interested in situations where the dimension  $N \in \mathbb{N}$  of the state  $\mathbf{x}(\boldsymbol{\xi})$  is high, which means that the system eq. (1) is potentially expensive to solve numerically, especially if these simulations need to be repeated for many parameter samples in outer-loop applications [39] such as optimization, uncertainty quantification, and control.

A common approach to constructing a reduced model of the full system eq. (1) is to use projection-based model reduction [9]. Towards this goal, let the columns of the matrix  $\mathbf{X} = [\mathbf{x}_1, \dots, \mathbf{x}_M] \in \mathbb{R}^{N \times M}$  be  $M \in \mathbb{N}$  snapshots derived from the parameter samples  $\boldsymbol{\xi}_1, \dots, \boldsymbol{\xi}_M \in \mathcal{D}$  such that  $\mathbf{x}_i = \mathbf{x}(\boldsymbol{\xi}_i)$  for  $i = 1, \dots, M$ . Further, let  $\mathbf{V} = [\mathbf{v}_1, \dots, \mathbf{v}_r] \in \mathbb{R}^{N \times r}$  be an  $r$ -dimensional orthonormal basis constructed from the snapshot matrix  $\mathbf{X}$ . The usual approach to obtaining  $\mathbf{V}$  is to compute the singular value decomposition (SVD) of  $\mathbf{X}$  and then to define  $\mathbf{V}$  as the leading  $r$  left singular vectors, as done in proper orthogonal decomposition (POD). Then, the POD-Galerkin reduced system is obtained via projection

$$\tilde{\mathbf{A}}\tilde{\mathbf{x}}(\boldsymbol{\xi}) + \mathbf{V}^T \mathbf{f}(\mathbf{V}\tilde{\mathbf{x}}(\boldsymbol{\xi}); \boldsymbol{\xi}) = 0, \quad (2)$$

where  $\tilde{\mathbf{A}} = \mathbf{V}^T \mathbf{A} \mathbf{V}$  is the reduced linear operator and  $\tilde{\mathbf{x}}(\boldsymbol{\xi}) \in \mathbb{R}^r$  is the reduced state.

Even though the reduced state  $\tilde{\mathbf{x}}(\boldsymbol{\xi})$  evolves in the  $r$ -dimensional subspace, evolution of the reduced nonlinear term  $\mathbf{V}^T \mathbf{f}(\mathbf{V}\tilde{\mathbf{x}}(\boldsymbol{\xi}); \boldsymbol{\xi})$  in eq. (2) still requires, first, lifting  $\tilde{\mathbf{x}}(\boldsymbol{\xi})$  to the full dimension  $N$ , evaluating the original nonlinear term in this original dimension, and then projecting it down to the reduced dimension; thus, evaluating the reduced model eq. (2) still requires operations that scale with the dimension of the full model. This is called the lifting bottleneck in nonlinear model reduction.

An effective remedy to the lifting bottleneck is the empirical interpolation method [7, 17]. The goal is to find an accurate approximation  $\tilde{\mathbf{f}}$  to  $\mathbf{f}$  that is computationally cheap to evaluate with cost independent of the dimension  $N$ . The empirical interpolation approximant  $\tilde{\mathbf{f}}$  has the form

$$\tilde{\mathbf{f}}(\mathbf{x}) = \mathbf{U}\mathbf{c}(\mathbf{x}) \quad (3)$$

where the columns of  $\mathbf{U} \in \mathbb{R}^{N \times n}$  form a basis of a space in which to approximate the function  $\mathbf{f}$  with  $n \ll N$  and the coefficients  $\mathbf{c}(\mathbf{x}) \in \mathbb{R}^n$  define the linear combination of the basis vectors that approximates  $\mathbf{f}(\mathbf{x})$ . DEIM achieves the approximation  $\tilde{\mathbf{f}}$  by interpolating  $\mathbf{f}$  at selected components. Let  $p_1, \dots, p_n \in \{1, \dots, N\}$  be the interpolation points (indices), i.e.,  $\mathbf{e}_{p_i}^T \mathbf{f}(\mathbf{x}) = \mathbf{e}_{p_i}^T \tilde{\mathbf{f}}(\mathbf{x})$  for  $i = 1, 2, \dots, n$ , where  $\mathbf{e}_i \in \mathbb{R}^N$  denotes the  $i$ -th canonical unit vector. Let  $\mathbf{P} = [\mathbf{e}_{p_1}, \dots, \mathbf{e}_{p_n}] \in \mathbb{R}^{N \times n}$  be the corresponding interpolation points (index selection) matrix. Then, the interpolation conditions are  $\mathbf{P}^T \mathbf{f}(\mathbf{x}) = \mathbf{P}^T \tilde{\mathbf{f}}(\mathbf{x})$ , which, using eq. (3), lead to

$$\tilde{\mathbf{f}}(\mathbf{x}) = \mathbf{U}\mathbf{c}(\mathbf{x}) = \mathbf{U}(\mathbf{P}^T \mathbf{U})^{-1} \mathbf{P}^T \mathbf{f}(\mathbf{x}), \quad (4)$$

---

**Algorithm 1** Interpolation points selection with QDEIM
 

---

```

1: procedure QDEIM( $\mathbf{U}$ )
2:    $n = \text{size}(\mathbf{U}, 2)$ 
3:    $[\sim, \sim, \phi] = \text{qr}(\mathbf{U}^T, \text{'vector'})$ 
4:    $\phi = \phi[1 : n]$ 
5: return  $\phi$ 
6: end procedure
  
```

---

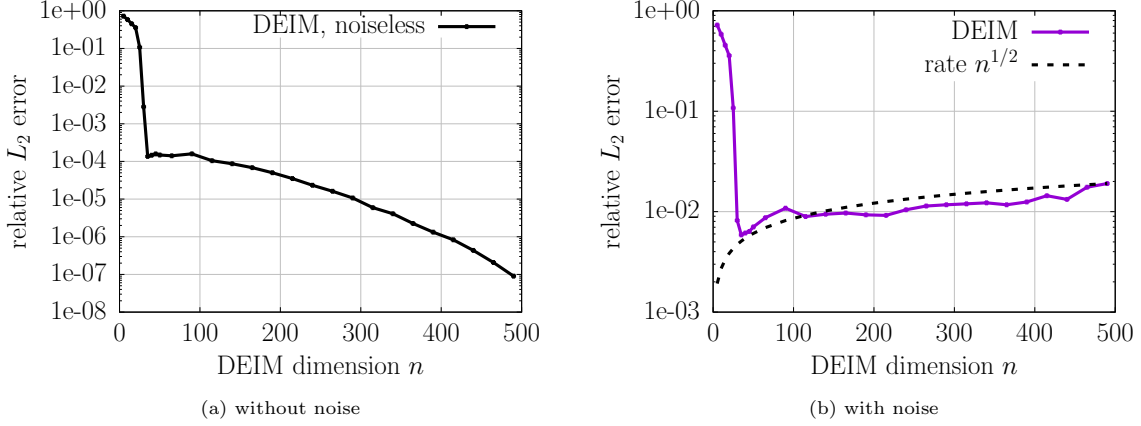


Figure 1: The DEIM is sensitive to noise in the sparse samples of the nonlinear function. In particular, the noise is amplified as the dimension of the DEIM space is increased. A rate of  $\sqrt{n}$  is numerically observed. We investigate oversampling DEIM to avoid the amplification of noise.

where  $\mathbf{c}(\mathbf{x}) = (\mathbf{P}^T \mathbf{U})^{-1} \mathbf{P}^T \mathbf{f}(\mathbf{x})$ . In eq. (4),  $\tilde{\mathbf{f}}$  is the DEIM approximation of  $\mathbf{f}$ .

The columns of  $\mathbf{U} \in \mathbb{R}^{N \times n}$  are usually taken as the POD basis of the nonlinear snapshots  $\mathbf{f}(\mathbf{x}_1), \mathbf{f}(\mathbf{x}_2), \dots, \mathbf{f}(\mathbf{x}_M)$ . Note that  $\mathbf{U}$  is orthonormal. The choice of the selection operator  $\mathbf{P}$ , is motivated by the error expression

$$\|\mathbf{f} - \tilde{\mathbf{f}}\|_2 \leq \|(\mathbf{P}^T \mathbf{U})^{-1}\|_2 \|(\mathbf{I} - \mathbf{U}\mathbf{U}^T)\mathbf{f}\|_2, \quad (5)$$

where  $\|(\mathbf{I} - \mathbf{U}\mathbf{U}^T)\mathbf{f}\|_2$  is the error due to the optimal approximation by orthogonal projection. Therefore, the selection operator  $\mathbf{P}$  should choose indices such that  $\|(\mathbf{P}^T \mathbf{U})^{-1}\|_2$  is small. The DEIM algorithm [7, 17] performs a greedy search to select the interpolation points. The QDEIM point selection algorithm [22, 23] based on the rank-revealing QR factorization is an alternative to this greedy-based point selection algorithms and returns quasi-optimal interpolation points in the sense that we will make precise below. We will use QDEIM for selecting interpolation points in the following, see Algorithm 1. Combining the DEIM approximation eq. (4) with the POD-Galerkin reduced model eq. (2), we obtain the POD-DEIM-Galerkin reduced system

$$\tilde{\mathbf{A}}\tilde{\mathbf{x}}(\boldsymbol{\xi}) + \mathbf{V}^T \mathbf{U} (\mathbf{P}^T \mathbf{U})^{-1} \mathbf{P}^T \mathbf{f}(\mathbf{V}\tilde{\mathbf{x}}(\boldsymbol{\xi}); \boldsymbol{\xi}) = 0, \quad (6)$$

where the  $N - n$  components of  $\mathbf{f}(\mathbf{V}\tilde{\mathbf{x}}(\boldsymbol{\xi}); \boldsymbol{\xi})$  that are different from the interpolation points  $p_1, \dots, p_n$  are approximated via empirical interpolation. Thus, the reduced system eq. (6) requires evaluating the nonlinear function  $\mathbf{f}$  at only  $n$  components, which typically leads to significant speedups compared to the POD-Galerkin reduced system eq. (2) that requires evaluating the function  $\mathbf{f}$  at all  $N$  components.

## 2.2 Instability of empirical interpolation in the presence of noise

To approximate  $\mathbf{f}(\mathbf{V}\tilde{\mathbf{x}}(\boldsymbol{\xi}); \boldsymbol{\xi})$  with DEIM in the reduced system eq. (6), the function  $\mathbf{f}$  is evaluated (at least) at the components of  $\mathbf{V}\tilde{\mathbf{x}}(\boldsymbol{\xi})$  corresponding to the interpolation points  $p_1, \dots, p_n$ , while all the other components are approximated via interpolation in the DEIM space spanned by the columns of the basis matrix  $\mathbf{U}$ . We are interested in the situation where the function evaluations of  $\mathbf{f}$  at  $\mathbf{V}\tilde{\mathbf{x}}(\boldsymbol{\xi})$  are noisy, in which case DEIM approximations can become unstable, as demonstrated in, e.g., [2].

Consider the parametrized nonlinear function

$$\mathbf{f}(\mathbf{x}; \xi) = 10^{-4}\xi (\sin(\xi\mathbf{x}) + \sin(\xi 2\pi\mathbf{x}) + \sin(\mathbf{x}\xi\pi)) + 10^{-6} \exp\left(-\frac{(\mathbf{x} - \xi)^2}{5 \times 10^{-5}}\right), \quad (7)$$

with the parameter  $\xi \in \mathcal{D} = [1, 3] \subset \mathbb{R}$ . The components of  $\mathbf{x} \in \mathbb{R}^{8192}$  are the equidistant points in  $\Omega = [-2\pi, 2\pi]$ . Note that all operations in eq. (7) are to be understood component-wise. Let  $\xi_1, \dots, \xi_{2500}$  be the equidistant points in  $\mathcal{D}$  and let  $\mathbf{f}(\mathbf{x}; \xi_1), \dots, \mathbf{f}(\mathbf{x}; \xi_{2500})$  be the nonlinear snapshots to derive a DEIM interpolant  $\tilde{\mathbf{f}}$  of  $\mathbf{f}$  of dimension  $n$  with the DEIM basis matrix  $\mathbf{U}$  and the DEIM interpolation points matrix  $\mathbf{P}$  obtained with the greedy algorithm [17, Algorithm 1]. We now approximate the function  $\mathbf{f}$  at the 2500 parameters  $\xi'_1, \dots, \xi'_{2500} \in \mathcal{D}$  uniformly sampled parameters in the domain  $\mathcal{D}$ . The DEIM approximation  $\tilde{\mathbf{f}}$  of  $\mathbf{f}$  is

$$\tilde{\mathbf{f}}(\mathbf{x}; \xi'_i) = \mathbf{U}(\mathbf{P}^T \mathbf{U})^{-1} \mathbf{P}^T \mathbf{f}(\mathbf{x}; \xi_i),$$

for  $i = 1, \dots, 2500$ . The averaged relative  $L_2$  error

$$\frac{1}{2500} \sum_{i=1}^{2500} \frac{\|\mathbf{f}(\mathbf{x}; \xi'_i) - \tilde{\mathbf{f}}(\mathbf{x}; \xi'_i)\|_2}{\|\mathbf{f}(\mathbf{x}; \xi'_i)\|_2} \quad (8)$$

versus the dimension  $n$  of the DEIM approximation is plotted in Figure 1a. The results indicate a fast decay of the DEIM approximation error with the dimension  $n$ .

Let us now consider noisy evaluations of the function  $\mathbf{f}$ . Therefore, let  $\boldsymbol{\epsilon}$  be a random vector that has, as components, independent zero-mean Gaussian random variables with standard deviation  $\sigma = 10^{-6}$ . Define

$$\mathbf{f}_\epsilon(\mathbf{x}; \xi) = \mathbf{f}(\mathbf{x}; \xi) + \boldsymbol{\epsilon}, \quad (9)$$

so that the DEIM approximation using the noisy function evaluations eq. (9) is

$$\tilde{\mathbf{f}}_\epsilon(\mathbf{x}; \xi) = \mathbf{U}(\mathbf{P}^T \mathbf{U})^{-1} \mathbf{P}^T \mathbf{f}_\epsilon(\mathbf{x}; \xi).$$

The plot in Figure 1b shows the averaged relative  $L_2$  error of the DEIM approximation  $\tilde{\mathbf{f}}_\epsilon$  that is derived from the noisy function evaluations eq. (9). The results indicate a stability issue of DEIM in this case of noisy function evaluations because the error grows with the dimension  $n$  of the DEIM space. The result illustrates an error growth with a rate  $\sqrt{n}$  with the dimension  $n$ . Similar observations are made in [2].

## 3 Amplification of noise in DEIM

We provide an upper bound on the amplification of the noise in DEIM approximations, a theoretical explanation of the numerical observation in Figure 1b. The bound eq. (11) shows that the error cannot increase faster than with rate  $\sqrt{n}$ , the rate observed in Figure 1b. A similar bound to eq. (11) has been presented in [2]. Here we also provide a formula for the expected value of the DEIM error vector and reveal the structure of the error ellipsoid.

To simplify the exposition, we drop the dependence on the spatial coordinate  $\mathbf{x}$  and the parameter  $\boldsymbol{\xi}$  of  $\mathbf{f}(\mathbf{x}; \boldsymbol{\xi})$ , and abbreviate it as  $\mathbf{f}(\mathbf{x}; \boldsymbol{\xi}) = \mathbf{f}$ . Similarly, the DEIM approximant will be abbreviated as  $\tilde{\mathbf{f}}$ . The noisy counterparts of  $\mathbf{f}$  and  $\tilde{\mathbf{f}}$  are  $\mathbf{f}_\epsilon = \mathbf{f} + \boldsymbol{\epsilon}$  and  $\tilde{\mathbf{f}}_\epsilon$ , respectively, where  $\boldsymbol{\epsilon}$  is a zero-mean Gaussian vector with independent components with standard deviation  $\boldsymbol{\sigma} = [\sigma_1, \dots, \sigma_N]^T$ .

**Lemma 3.1.** Define the DEIM error of the DEIM approximation  $\tilde{\mathbf{f}}_\epsilon$  from noisy function evaluations as  $\mathbf{r}_\epsilon = \mathbf{f} - \tilde{\mathbf{f}}_\epsilon = \mathbf{f} - \mathbf{U}(\mathbf{P}^T \mathbf{U})^{-1} \mathbf{P}^T \mathbf{f}_\epsilon$  and the error of the approximation  $\tilde{\mathbf{f}}$  with noise-free function evaluations as  $\mathbf{r} = \mathbf{f} - \mathbf{U}(\mathbf{P}^T \mathbf{U})^{-1} \mathbf{P}^T \mathbf{f}$ . Then, the expected value of the error  $\mathbf{r}_\epsilon$  corresponding to noisy function evaluations equals  $\mathbf{r}$ , i.e.,  $\mathbb{E}_\epsilon[\mathbf{r}_\epsilon] = \mathbf{r}$ , where the expectation is taken over the noise. The standard deviation of  $\mathbf{r}_\epsilon$  is

$$\mathbb{E}_\epsilon [\|\mathbf{r}_\epsilon - \mathbb{E}_\epsilon[\mathbf{r}_\epsilon]\|_2] \leq \sqrt{\mathbb{E}_\epsilon [\|\mathbf{r}_\epsilon - \mathbb{E}_\epsilon[\mathbf{r}_\epsilon]\|_2^2]} \leq \sqrt{n} \|(\mathbf{P}^T \mathbf{U})^{-1}\|_2 \|\mathbf{P}^T \boldsymbol{\sigma}\|_\infty. \quad (10)$$

Thus, the error is bounded in expectation as

$$\mathbb{E}_\epsilon [\|\mathbf{f} - \mathbf{U}(\mathbf{P}^T \mathbf{U})^{-1} \mathbf{P}^T \mathbf{f}_\epsilon\|_2] \leq \|(\mathbf{P}^T \mathbf{U})^{-1}\|_2 (\|\mathbf{f} - \mathbf{U} \mathbf{U}^T \mathbf{f}\|_2 + \sqrt{n} \|\mathbf{P}^T \boldsymbol{\sigma}\|_\infty). \quad (11)$$

*Proof.* Using the linearity of the expectation, the error formula for the DEIM projection, the assumptions on the noise, namely,  $\mathbb{E}_\epsilon[\boldsymbol{\epsilon}] = 0$ , we obtain

$$\begin{aligned} \mathbb{E}_\epsilon [\mathbf{f} - \mathbf{U}(\mathbf{P}^T \mathbf{U})^{-1} \mathbf{P}^T \mathbf{f}_\epsilon] &= (\mathbf{I} - \mathbf{U}(\mathbf{P}^T \mathbf{U})^{-1} \mathbf{P}^T) \mathbf{f} - \mathbf{U}(\mathbf{P}^T \mathbf{U})^{-1} \mathbf{P}^T \mathbb{E}_\epsilon[\boldsymbol{\epsilon}] \\ &= (\mathbf{I} - \mathbf{U}(\mathbf{P}^T \mathbf{U})^{-1} \mathbf{P}^T) \mathbf{f}, \end{aligned} \quad (12)$$

which establishes  $\mathbb{E}_\epsilon[\mathbf{r}_\epsilon] = \mathbf{r}$  as claimed. The norm of  $\|\mathbb{E}_\epsilon[\mathbf{r}_\epsilon]\|_2$  is bounded as

$$\|\mathbb{E}_\epsilon [\mathbf{f} - \mathbf{U}(\mathbf{P}^T \mathbf{U})^{-1} \mathbf{P}^T \mathbf{f}_\epsilon]\|_2 \leq \|(\mathbf{P}^T \mathbf{U})^{-1}\|_2 \|\mathbf{f} - \mathbf{U} \mathbf{U}^T \mathbf{f}\|_2. \quad (13)$$

The covariance matrix of the error  $\mathbf{r}_\epsilon$  is

$$\begin{aligned} \mathbf{C} &= \mathbb{E}_\epsilon [\mathbf{U}(\mathbf{P}^T \mathbf{U})^{-1} \mathbf{P}^T \boldsymbol{\epsilon} \boldsymbol{\epsilon}^T \mathbf{P}(\mathbf{P}^T \mathbf{U})^{-T} \mathbf{U}^T] = \mathbf{U}(\mathbf{P}^T \mathbf{U})^{-1} \mathbf{P}^T \Sigma^2 \mathbf{P}(\mathbf{P}^T \mathbf{U})^{-T} \mathbf{U}^T \\ &= \mathbf{U}(\mathbf{P}^T \mathbf{U})^{-1} \Sigma_{\mathbf{P}}^2 (\mathbf{P}^T \mathbf{U})^{-T} \mathbf{U}^T, \end{aligned}$$

where  $\Sigma_{\mathbf{P}} = \mathbf{P}^T \Sigma \mathbf{P} = \text{diag}(\sigma_{p_i})_{i=1}^n$  with  $\sigma_{p_i}$  being the standard deviation of the  $p_i$ -th component of  $\boldsymbol{\epsilon}$ . The covariance  $\mathbf{C}$  is positive semidefinite. Its nonzero eigenvalues  $\lambda_i^2$  (that correspond to the invariant space spanned by  $\mathbf{U}$ ) can be enumerated so that

$$\lambda_i^2 = \sigma_{p_i}^2 \vartheta_i^2, \quad \text{where} \quad \frac{1}{\|(\mathbf{P}^T \mathbf{U})^{-1}\|_2} \leq \vartheta_i \leq \|(\mathbf{P}^T \mathbf{U})^{-1}\|_2, \quad i = 1, \dots, n.$$

This is an application of the Ostrowski theorem [29, Theorem 4.5.9]; it identifies the bounds of the amplification factors  $\vartheta_i$ 's of the corresponding standard deviations. The spectral structure of  $\mathbf{C}$  (and thus the error ellipsoid) can be explicitly revealed using the SVD decomposition  $\Sigma_{\mathbf{P}}^{-1}(\mathbf{P}^T \mathbf{U}) = \Phi \Omega \Psi^T$  ( $\Phi, \Psi$  orthogonal matrices of singular vector,  $\Omega$  diagonal matrix of singular values), which yields  $\mathbf{C} = (\mathbf{U} \Psi) \Omega^{-2} (\mathbf{U} \Psi)^T$ .

Next, of interest is the variance  $\mathbb{E}_\epsilon[\|\mathbf{r}_\epsilon - \mathbb{E}_\epsilon[\mathbf{r}_\epsilon]\|_2^2]$  of  $\mathbf{r}_\epsilon$ , for which follows that

$$\mathbb{E}_\epsilon [\|\mathbf{r}_\epsilon - \mathbb{E}_\epsilon[\mathbf{r}_\epsilon]\|_2^2] = \text{Trace}(\mathbf{C}) = \sum_{i=1}^n \sigma_{p_i}^2 \vartheta_i^2 \leq n \|(\mathbf{P}^T \mathbf{U})^{-1}\|_2^2 \max_i \sigma_{p_i}^2,$$

which shows  $\mathbb{E}_\epsilon [\|\mathbf{r}_\epsilon - \mathbb{E}_\epsilon[\mathbf{r}_\epsilon]\|_2^2] \leq n \|\mathbf{P}^T \boldsymbol{\sigma}\|_\infty^2 \|(\mathbf{P}^T \mathbf{U})^{-1}\|_2^2$ . In addition, by deploying the Jensen's inequality and taking square root, we have obtain eq. (10). Then, combining the above estimates and the triangle inequality yields

$$\begin{aligned} \mathbb{E}_\epsilon [\|\mathbf{r}_\epsilon\|_2] &\leq \mathbb{E}_\epsilon [\|\mathbf{r}_\epsilon - \mathbb{E}_\epsilon[\mathbf{r}_\epsilon]\|_2] + \|\mathbb{E}_\epsilon[\mathbf{r}_\epsilon]\|_2 \\ &\leq \|(\mathbf{P}^T \mathbf{U})^{-1}\|_2 (\|\mathbf{f} - \mathbf{U} \mathbf{U}^T \mathbf{f}\|_2 + \sqrt{n} \|\mathbf{P}^T \boldsymbol{\sigma}\|_\infty). \end{aligned}$$

which proves eq. (11). □

**Corollary 3.2.** *If the selection operator  $\mathbf{P}$  is based on the quasi-optimal point selection introduced in [23, Lemma 2.1], then eq. (10) and eq. (11) hold with the bound*

$$\|(\mathbf{P}^T \mathbf{U})^{-1}\|_2 \leq \sqrt{1 + \eta^2 n(N - n)}. \quad (14)$$

where  $\eta \geq 1$  is a tuning parameter.

**Remark 3.3.** Note how in eq. (11), with increasing column dimension  $n$  of the matrix  $\mathbf{U}$ , the POD projection error monotonically decreases toward zero and, at the same time, the condition number  $\|(\mathbf{P}^T \mathbf{U})^{-1}\|_2$  monotonically approaches one, while the contribution of the noise grows as  $\sqrt{n}\|\mathbf{P}^T \boldsymbol{\sigma}\|_\infty$ , taking over the leading term. The effect of the noise dominating the error is seen in Figure 1.

**Remark 3.4.** From Lemma 3.1, it follows that it is desirable to avoid components of  $\mathbf{f}$  with noise with high variance, i.e., the DEIM selection operator should avoid them. Such a strategy may help slow the noise buildup. If we denote by  $\mathcal{J}$  undesirable indices and set  $\mathcal{J}^c = \{1, \dots, N\} \setminus \mathcal{J}$ , then we can run the QDEIM selection on the submatrix  $\mathbf{U}(\mathcal{J}^c, :)$ ; for details we refer the reader to [22, §3].

## 4 Oversampled DEIM (ODEIM)

Given the DEIM basis  $\mathbf{U} \in \mathbb{R}^{N \times n}$ , the classical DEIM selects  $n$  interpolation points, i.e.,  $\mathbf{P}^T \mathbf{U}$  is a square matrix. In this section, we investigate oversampling for DEIM (ODEIM) to obtain the discrete empirical regression method and show that the noise amplification, observed and proved in Section 3, can be avoided with ODEIM in expectation with high probability. Note that oversampling for DEIM has been proposed in the literature, see Section 1.

### 4.1 ODEIM

Consider  $p_1, \dots, p_m \in \{1, \dots, N\}$ , pairwise distinct sampling points with  $m > n$ , i.e., the number of sampling points  $m$  is larger than the dimension  $n$  of the DEIM space spanned by the columns of the DEIM basis matrix  $\mathbf{U}$ . Then, the corresponding ODEIM approximation of  $\mathbf{f}$  is

$$\hat{\mathbf{f}} = \mathbf{U}(\mathbf{P}^T \mathbf{U})^\dagger \mathbf{P}^T \mathbf{f},$$

where  $\mathbf{M}^\dagger$  denotes the Moore-Penrose inverse of  $\mathbf{M}$ , i.e.,  $\mathbf{M}^\dagger = (\mathbf{M}^T \mathbf{M})^{-1} \mathbf{M}^T$ , assuming  $\mathbf{M}$  has linearly independent columns. In contrast to the DEIM approximation  $\tilde{\mathbf{f}}$  in eq. (4), the ODEIM approximation  $\hat{\mathbf{f}}$  is obtained via regression and therefore does not necessarily interpolate  $\mathbf{f}$  at the sampling points  $p_1, \dots, p_m$ . In the case of noise-free sampling, the  $L_2$  error of the ODEIM approximation satisfies

$$\|\mathbf{f} - \hat{\mathbf{f}}\|_2 \leq \|(\mathbf{P}^T \mathbf{U})^\dagger\|_2 \|\mathbf{f} - \mathbf{U} \mathbf{U}^T \mathbf{f}\|_2, \quad (15)$$

where  $\|(\mathbf{P}^T \mathbf{U})^\dagger\|_2$  quantifies the effect of the sampling points and  $\|\mathbf{f} - \mathbf{U} \mathbf{U}^T \mathbf{f}\|_2$  the approximation quality of the space spanned by  $\mathbf{U}$ , as in the DEIM error bound eq. (5).

### 4.2 Probabilistic analysis of ODEIM

We now investigate the error of the ODEIM approximation  $\hat{\mathbf{f}}$  when the sampling points  $p_1, \dots, p_m$  are selected uniformly with replacement from  $\{1, \dots, N\}$ . Note that the following analysis is developed for uniform sampling *with replacement* as in the work by Balzano et al. [6]. Parts of the following analysis are an application of the work by Cohen et al. [20].

To set up the analysis, we define the coherence of a subspace  $\mathcal{U} = \text{span}(\mathbf{U})$  as

$$\mu(\mathcal{U}) = \frac{N}{n} \max_{i=1, \dots, N} \|\mathbf{u}_i^T\|_2^2,$$

where the columns of  $\mathbf{U} \in \mathbb{R}^{N \times n}$  are an orthonormal basis of  $\mathcal{U}$  and  $\mathbf{u}_i^T$  is the  $i$ -th row of  $\mathbf{U}$ , see, e.g., [13, Definition 1.2]. Note that  $\max_{i=1, \dots, N} \|\mathbf{u}_i^T\|_2^2 \geq n/N$ . The following result from [6, Lemma 3] will be used in our analysis.

**Lemma 4.1.** *Let the points  $p_1, \dots, p_m$  be uniformly sampled from  $\{1, \dots, N\}$  with replacement and let  $\mathbf{P}$  be the corresponding sampling points matrix. Let further  $\delta > 0$ ,  $m \geq (8/3)n\mu(\mathcal{U}) \log(2n/\delta)$ , and set  $\gamma = \sqrt{\frac{8n\mu(\mathcal{U})}{3m}} \log(2n/\delta)$ . Then*

$$\left\| \left( (\mathbf{P}^T \mathbf{U})^T (\mathbf{P}^T \mathbf{U}) \right)^{-1} \right\|_2 \leq \frac{N}{(1-\gamma)m}$$

with probability at least  $1 - \delta$ .

The following lemma states that  $\|(\mathbf{P}^T \mathbf{U})^\dagger\|_2$  can be bounded by a (small) constant with high probability if a sufficiently large number of sampling points is used, which means that ODEIM is well-posed with high probability.

**Lemma 4.2.** *Consider the same setup as in Lemma 4.1 and set  $\hat{\gamma} = \sqrt{m}\gamma$ . If  $m$  is such that*

$$\sqrt{m} \geq \frac{1}{2}\hat{\gamma} + \frac{1}{2}\sqrt{\hat{\gamma}^2 + \frac{4N}{K^2}}, \quad (16)$$

then

$$\|(\mathbf{P}^T \mathbf{U})^\dagger\|_2 \leq K,$$

with probability at least  $1 - \delta$ .

*Proof.* Since  $\|(\mathbf{P}^T \mathbf{U})^\dagger\|_2 = \sqrt{\|(\mathbf{P}^T \mathbf{U})^T (\mathbf{P}^T \mathbf{U})\|_2^{-1}}$ , Lemma 4.1 yields

$$\|(\mathbf{P}^T \mathbf{U})^\dagger\|_2 \leq \sqrt{\frac{N}{(1-\gamma)m}}. \quad (17)$$

Then, the task is to choose  $m$  so that  $N/((1-\gamma)m) \leq K^2$ . To that end, set  $\hat{\gamma} = \sqrt{m}\gamma$ . By the assumption of Lemma 4.1,  $\sqrt{m} \geq \hat{\gamma}$ . The desired inequality becomes

$$N \leq K^2(m - \sqrt{m}\hat{\gamma}), \quad \text{i.e., } K^2x^2 - K^2\hat{\gamma}x - N \geq 0, \quad \text{where } x = \sqrt{m} \geq \hat{\gamma}.$$

The smaller root of the above parabola is negative and the larger one, then, provides the desired lower bound eq. (16).  $\square$

The following bound will be helpful in establishing the main result.

**Lemma 4.3.** *Consider the same setup as in Lemma 4.1. Let  $\mathbf{g} \in \mathbb{R}^N$ , and let  $\alpha$  be the acute angle between  $\mathbf{g}$  and the range of  $\mathbf{U}$ . Then,*

$$\mathbb{E}_{\mathcal{P}} \left[ \|(\mathbf{P}^T \mathbf{U})^\dagger \mathbf{P}^T \mathbf{g}\|_2 \right] \leq \min \left\{ \frac{1}{\sqrt{1-\gamma}}, \frac{\sqrt{\cos^2 \alpha + \frac{n}{m}\mu(\mathcal{U})}}{1-\gamma} \right\} \|\mathbf{g}\|_2 \quad (18)$$

with probability at least  $1 - \delta$ , where the expected value  $\mathbb{E}_{\mathcal{P}}$  is with respect to the uniform distribution of the sampling points.

*Proof.* We first apply submultiplicativity to obtain

$$\|(\mathbf{P}^T \mathbf{U})^\dagger \mathbf{P}^T \mathbf{g}\|_2 \leq \|(\mathbf{P}^T \mathbf{U})^\dagger\|_2 \|\mathbf{P}^T \mathbf{g}\|_2. \quad (19)$$

Using eq. (17) and Lemma 4.1, we have, with probability at least  $1 - \delta$ , that

$$\mathbb{E}_P [\|(\mathbf{P}^T \mathbf{U})^\dagger\|_2 \|\mathbf{P}^T \mathbf{g}\|_2] \leq \sqrt{\frac{N}{(1-\gamma)m}} \mathbb{E}_P [\|\mathbf{P}^T \mathbf{g}\|_2]. \quad (20)$$

Consider now the expected value  $\mathbb{E}_P[\|\mathbf{P}^T \mathbf{g}\|_2^2]$  and note that we use the squared Euclidean norm  $\|\cdot\|_2^2$ . Let  $g_j$  denote the  $j$ -th component of  $\mathbf{g}$  for  $j = 1, \dots, N$ . Also let  $\mathbb{I}_{p_i=j}$  denote the indicator function that is 1 if  $p_i = j$  and 0 otherwise. Note that the probability that  $p_i = j$  is  $\mathbb{P}_P[\mathbb{I}_{j=p_i}] = 1/N$  because a uniform distribution with replacement is used for selecting the sampling points, and thus  $\mathbb{E}[\mathbb{I}_{p_i=j}] = 1/N$ . Then,

$$\mathbb{E}_P [\|\mathbf{P}^T \mathbf{g}\|_2^2] = \mathbb{E}_P \left[ \sum_{i=1}^m \sum_{j=1}^N g_j^2 \mathbb{I}_{p_i=j} \right] = \frac{m}{N} \|\mathbf{g}\|_2^2. \quad (21)$$

Applying Jensen's inequality to eq. (21) yields  $\mathbb{E}_P[\|\mathbf{P}^T \mathbf{g}\|_2] \leq \sqrt{\frac{m}{N}} \|\mathbf{g}\|_2$ , which, combined with eq. (20) implies

$$\mathbb{E}_P [\|(\mathbf{P}^T \mathbf{U})^\dagger \mathbf{P}^T \mathbf{g}\|_2] \leq \frac{1}{\sqrt{1-\gamma}} \|\mathbf{g}\|_2, \quad (22)$$

proving the upper bound in eq. (18) for the first input of the min function. To prove eq. (18) for the second input of the min function, we first apply submultiplicativity to obtain

$$\|(\mathbf{P}^T \mathbf{U})^\dagger \mathbf{P}^T \mathbf{g}\|_2 \leq \left\| ((\mathbf{P}^T \mathbf{U})^T (\mathbf{P}^T \mathbf{U}))^{-1} \right\|_2 \|(\mathbf{P}^T \mathbf{U})^T \mathbf{P}^T \mathbf{g}\|_2. \quad (23)$$

With Lemma 4.1, we have, with probability at least  $1 - \delta$ , that

$$\begin{aligned} \mathbb{E}_P \left[ \left\| ((\mathbf{P}^T \mathbf{U})^T (\mathbf{P}^T \mathbf{U}))^{-1} \right\|_2 \|(\mathbf{P}^T \mathbf{U})^T \mathbf{P}^T \mathbf{g}\|_2 \right] \\ \leq \frac{N}{(1-\gamma)m} \mathbb{E}_P [\|(\mathbf{P}^T \mathbf{U})^T \mathbf{P}^T \mathbf{g}\|_2]. \end{aligned} \quad (24)$$

Let  $\langle \mathbf{v}, \mathbf{w} \rangle_2 = \mathbf{v}^T \mathbf{w}$  denote the Euclidean inner product and consider the expected value  $\mathbb{E}_P[\|(\mathbf{P}^T \mathbf{U})^T \mathbf{P}^T \mathbf{g}\|_2^2]$ .

$$\begin{aligned} \mathbb{E}_P[\langle (\mathbf{P}^T \mathbf{U})^T \mathbf{P}^T \mathbf{g}, (\mathbf{P}^T \mathbf{U})^T \mathbf{P}^T \mathbf{g} \rangle_2] &= \mathbb{E}_P \left[ \sum_{j=1}^m \sum_{k=1}^m \langle g_{p_j} \mathbf{u}_{p_j}^T, g_{p_k} \mathbf{u}_{p_k}^T \rangle_2 \right] \\ &= \mathbb{E}_P \left[ \sum_{j=1}^m \sum_{k=1}^m \left\langle \sum_{\ell=1}^N g_\ell \mathbf{u}_\ell^T \mathbb{I}_{p_j=\ell}, \sum_{s=1}^N g_s \mathbf{u}_s^T \mathbb{I}_{p_k=s} \right\rangle_2 \right] \\ &= \sum_{j=1}^m \sum_{k=1}^m \sum_{\ell=1}^N \sum_{s=1}^N g_\ell g_s \langle \mathbf{u}_\ell^T, \mathbf{u}_s^T \rangle_2 \mathbb{E}_P [\mathbb{I}_{p_j=\ell} \mathbb{I}_{p_k=s}] \end{aligned} \quad (25)$$

where in obtaining the last equality we used the linearity of  $\langle \cdot, \cdot \rangle_2$  and  $\mathbb{E}_P[\cdot]$ . Note that, for  $k \neq j$ , by independence of the  $j$ th and the  $k$ th drawing with replacement

$$\mathbb{E}_P [\mathbb{I}_{p_j=\ell} \mathbb{I}_{p_k=s}] = \frac{1}{N^2}. \quad (26)$$

Now we can use eq. (26) to split (25). For  $k \neq j$ , we obtain

$$\sum_{j=1}^m \sum_{\substack{k=1 \\ k \neq j}}^m \sum_{\ell=1}^N \sum_{s=1}^N g_\ell g_s \langle \mathbf{u}_\ell^T, \mathbf{u}_s^T \rangle_2 \frac{1}{N^2} = \frac{m^2 - m}{N^2} (\mathbf{U} \mathbf{U}^T \mathbf{g}, \mathbf{g})_2 = \frac{m^2 - m}{N^2} \|\mathbf{U} \mathbf{U}^T \mathbf{g}\|_2^2.$$

The remaining terms with  $j = k$  contribute to (25) with

$$\begin{aligned} \sum_{j=1}^m \sum_{\ell=1}^N \sum_{s=1}^N g_\ell g_s \langle \mathbf{u}_\ell^T, \mathbf{u}_s^T \rangle_2 \mathbb{E}_P [\mathbb{I}_{p_j=\ell} \mathbb{I}_{p_j=s}] &= \mathbb{E}_P \left[ \sum_{j=1}^m \sum_{\ell=1}^N g_\ell^2 \|\mathbf{u}_\ell^T\|_2^2 \mathbb{I}_{p_j=\ell} \right] \\ &= \frac{m}{N} \sum_{\ell=1}^N g_\ell^2 \|\mathbf{u}_\ell^T\|_2^2, \end{aligned}$$

where we use  $\mathbb{E}_P[\mathbb{I}_{p_j=\ell} \mathbb{I}_{p_j=s}] = 1/N$  for  $s = \ell$  and 0 otherwise. Altogether, we have

$$\begin{aligned} \mathbb{E}_P[\|(\mathbf{P}^T \mathbf{U})^T \mathbf{P}^T \mathbf{g}\|_2^2] &= \frac{m^2 - m}{N^2} \|\mathbf{U} \mathbf{U}^T \mathbf{g}\|_2^2 + \frac{m}{N} \|\text{diag}(\mathbf{g}) \mathbf{U}\|_F^2 \\ &= \frac{m^2 - m}{N^2} \|\mathbf{U} \mathbf{U}^T \mathbf{g}\|_2^2 + \frac{m}{N} \frac{n}{N} \mu(\mathcal{U}) \|\mathbf{g}\|_2^2 \quad (\text{here } \frac{n}{N} \mu(\mathcal{U}) = \max_{\ell=1, \dots, N} \|\mathbf{u}_\ell^T\|_2^2) \\ &= \frac{m^2 - m}{N^2} \|\mathbf{g}\|_2^2 \cos^2 \alpha + \frac{m}{N} \frac{n}{N} \mu(\mathcal{U}) \|\mathbf{g}\|_2^2, \end{aligned} \tag{27}$$

where  $\text{diag}(\mathbf{g}) \in \mathbb{R}^{N \times N}$  is the diagonal matrix with the components of  $\mathbf{g}$  on its diagonal. Hence, applying Jensen's inequality to (27) and then using eq. (24) yield

$$\mathbb{E}_P[\|(\mathbf{P}^T \mathbf{U})^\dagger \mathbf{P}^T \mathbf{g}\|_2] \leq \frac{\|\mathbf{g}\|_2}{1 - \gamma} \sqrt{\cos^2 \xi + \frac{n}{m} \mu(\mathcal{U})} = \frac{\|\mathbf{g}\|_2}{1 - \gamma} \sqrt{\cos^2 \xi + \frac{N}{m} \max_{\ell=1, \dots, N} \|\mathbf{u}_\ell^T\|_2^2}$$

Combining this final inequality with eq. (24) yields the desired result (18).  $\square$

**Remark 4.4.** The min function in the upper bound eq. (18) results from using two different upper bounds for  $\|(\mathbf{P}^T \mathbf{U})^\dagger \mathbf{P}^T \mathbf{g}\|_2$ , one as in eq. (19) and the other one as in eq. (23). The latter is employed by [6] for the special case where  $\mathbf{g}$  is orthogonal to the range of  $\mathbf{U}$ . While for small  $m$  values, the first input in the min function is expected to be smaller, as  $m$  increases, the second input is expected to be smaller. To provide a tighter bound for all cases, we choose to include both estimates in the bound.

**Remark 4.5.** If  $\mathbf{g}$  is orthogonal to the range of  $\mathbf{U}$ , in eq. (18) the term  $\cos \alpha = 0$  and the upper bound simplifies to

$$\mathbb{E}_P[\|(\mathbf{P}^T \mathbf{U})^\dagger \mathbf{P}^T \mathbf{g}\|_2] \leq \min \left\{ \frac{1}{\sqrt{1 - \gamma}}, \frac{\sqrt{\frac{n}{m} \mu(\mathcal{U})}}{1 - \gamma} \right\} \|\mathbf{g}\|_2.$$

Thus Lemma 4.3 contains [6, Lemma 2] as a special case. Indeed, in this special case, the expectation of  $(\mathbf{P}^T \mathbf{U})^T \mathbf{P}^T \mathbf{g}$  is zero because

$$\mathbb{E}_P[(\mathbf{P}^T \mathbf{U})^T \mathbf{P}^T \mathbf{g}] = \mathbb{E}_P \left[ \sum_{k=1}^m \sum_{j=1}^N \mathbf{u}_j^T g_j \mathbb{I}_{p_k=j} \right] = \frac{m}{N} \mathbf{U}^T \mathbf{g} = 0.$$

We now show that ODEIM is robust with respect to noise in the sense that increasing the number of sampling points  $m$  reduces the effect of the noise.

**Theorem 4.6.** Consider the same setup as in Lemma 4.1 and Lemma 4.3. Define

$$\zeta = \min \left\{ \frac{1}{\sqrt{1 - \gamma}}, \frac{1}{1 - \gamma} \sqrt{\frac{n}{m} \mu(\mathcal{U})} \right\}. \tag{28}$$

Then,

$$\mathbb{E}_P \left[ \mathbb{E}_\epsilon \left[ \|\mathbf{f} - \hat{\mathbf{f}}_\epsilon\|_2 \right] \right] \leq (1 + \zeta) \|\mathbf{f} - \mathbf{U} \mathbf{U}^T \mathbf{f}\|_2 + \frac{\|\boldsymbol{\sigma}\|_\infty}{(1 - \gamma)} \sqrt{\frac{nN}{m}} \tag{29}$$

with probability at least  $1 - \delta$ , where the expectation  $\mathbb{E}_P$  is with respect to the distribution of the samples and  $\mathbb{E}_\epsilon$  with respect to the noise in  $\mathbf{f}_\epsilon$  as defined in eq. (9).

*Proof.* We split the error following the strategy of [20, Theorem 2]. With the triangular inequality, we obtain

$$\mathbb{E}_P \left[ \mathbb{E}_\epsilon \left[ \|\mathbf{f} - \hat{\mathbf{f}}_\epsilon\|_2 \right] \right] \leq \mathbb{E}_P \left[ \|\mathbf{f} - \hat{\mathbf{f}}\|_2 \right] + \mathbb{E}_P \left[ \mathbb{E}_\epsilon \left[ \|\mathbf{U}(\mathbf{P}^T \mathbf{U})^\dagger \mathbf{P}^T \epsilon\|_2 \right] \right]. \quad (30)$$

with  $\hat{\mathbf{f}} = \mathbf{U}(\mathbf{P}^T \mathbf{U})^\dagger \mathbf{P}^T \mathbf{f}$  and  $\mathbf{f}_\epsilon = \mathbf{f} + \epsilon$ .

To bound the first term on the right-hand side of the inequality eq. (30), set  $\mathbf{g} = \mathbf{f} - \mathbf{U}\mathbf{U}^T \mathbf{f}$ . Similarly to the case in [17], it holds that

$$\mathbf{f} - \hat{\mathbf{f}} = \mathbf{f} - \mathbf{U}(\mathbf{P}^T \mathbf{U})^\dagger \mathbf{P}^T \mathbf{f} = \mathbf{g} - \mathbf{U}(\mathbf{P}^T \mathbf{U})^\dagger \mathbf{P}^T \mathbf{g}, \quad (31)$$

where we used the fact that  $(\mathbf{P}^T \mathbf{U})^\dagger \mathbf{P}^T \mathbf{U} = \mathbf{I}_n$  with probability, at least,  $1 - \delta$ . Note that  $\mathbf{g} = \mathbf{f} - \mathbf{U}\mathbf{U}^T \mathbf{f}$  is orthogonal to the range of  $\mathbf{U}$ . Then, Lemma 4.3 implies that

$$\mathbb{E}_P \left[ \|\mathbf{U}(\mathbf{P}^T \mathbf{U})^\dagger \mathbf{P}^T \mathbf{g}\|_2 \right] \leq \min \left\{ \frac{1}{\sqrt{1-\gamma}}, \frac{\sqrt{\frac{n}{m}\mu(\mathcal{U})}}{1-\gamma} \right\} \|\mathbf{g}\|_2 \quad (32)$$

with probability at least  $1 - \delta$ . Then, eq. (31) and the linearity of the expectation yield

$$\mathbb{E}_P \left[ \|\mathbf{f} - \hat{\mathbf{f}}\|_2 \right] \leq (1 + \zeta) \|\mathbf{f} - \mathbf{U}\mathbf{U}^T \mathbf{f}\|_2,$$

where  $\zeta$  is as defined in eq. (28). Now consider the second term on the right-hand side of eq. (30). Note that  $\epsilon$  is not necessarily orthogonal to  $\mathbf{U}$ , and therefore Remark 4.5 cannot be applied. We make the approximations

$$\mathbb{E}_P \left[ \mathbb{E}_\epsilon \left[ \|\mathbf{U}(\mathbf{P}^T \mathbf{U})^\dagger \mathbf{P}^T \epsilon\|_2 \right] \right] \leq \frac{N}{(1-\gamma)m} \mathbb{E}_P \left[ \mathbb{E}_\epsilon \left[ \|(\mathbf{P}^T \mathbf{U})^T \mathbf{P}^T \epsilon\|_2 \right] \right], \quad (33)$$

which holds with probability at least  $1 - \delta$ , see eq. (23) and eq. (24) in the proof of Lemma 4.3. Consider now  $\mathbb{E}_P \left[ \mathbb{E}_\epsilon \left[ \|(\mathbf{P}^T \mathbf{U})^T \mathbf{P}^T \epsilon\|_2^2 \right] \right]$ . With the same notation as in the proof of Lemma 4.3, and building on the proof of [20, Theorem 3], we have

$$\begin{aligned} & \mathbb{E}_P \left[ \mathbb{E}_\epsilon \left[ \|(\mathbf{P}^T \mathbf{U})^T \mathbf{P}^T \epsilon\|_2^2 \right] \right] = \mathbb{E}_P \left[ \mathbb{E}_\epsilon \left[ \langle (\mathbf{P}^T \mathbf{U})^T \mathbf{P}^T \epsilon, (\mathbf{P}^T \mathbf{U})^T \mathbf{P}^T \epsilon \rangle_2 \right] \right] \\ &= \mathbb{E}_P \left[ \mathbb{E}_\epsilon \left[ \left\langle \sum_{i=1}^m \epsilon_{p_i} \mathbf{u}_{p_i}^T, \sum_{j=1}^m \epsilon_{p_j} \mathbf{u}_{p_j}^T \right\rangle_2 \right] \right] = \mathbb{E}_P \left[ \sum_{i=1}^m \sum_{j=1}^m \mathbb{E}_\epsilon \left[ \langle \epsilon_{p_i} \mathbf{u}_{p_i}^T, \epsilon_{p_j} \mathbf{u}_{p_j}^T \rangle_2 \right] \right] \\ &= \mathbb{E}_P \left[ \sum_{i=1}^m \sum_{j=1}^m \mathbb{E}_\epsilon \left[ \epsilon_{p_i} \epsilon_{p_j} \langle \mathbf{u}_{p_i}^T, \mathbf{u}_{p_j}^T \rangle_2 \right] \right] = \mathbb{E}_P \left[ \sum_{i=1}^m \sum_{j=1}^m \mathbb{E}_\epsilon \left[ \epsilon_{p_i} \epsilon_{p_j} \right] \langle \mathbf{u}_{p_i}^T, \mathbf{u}_{p_j}^T \rangle_2 \right] \\ &= \mathbb{E}_P \left[ \sum_{i=1}^m \mathbb{E}_\epsilon \left[ \epsilon_{p_i}^2 \right] \langle \mathbf{u}_{p_i}^T, \mathbf{u}_{p_i}^T \rangle_2 \right] \quad (\text{since } \epsilon_{p_i} \text{ and } \epsilon_{p_j} \text{ are independent for } i \neq j) \\ &= \mathbb{E}_P \left[ \sum_{i=1}^m \sigma_{p_i}^2 \langle \mathbf{u}_{p_i}^T, \mathbf{u}_{p_i}^T \rangle_2 \right] = \mathbb{E}_P \left[ \sum_{i=1}^m \sum_{j=1}^N \sigma_j^2 \|\mathbf{u}_j^T\|_2^2 \mathbb{I}_{p_i=j} \right] = \frac{m}{N} \sum_{j=1}^N \sigma_j^2 \|\mathbf{u}_j^T\|_2^2. \end{aligned}$$

Using the fact that  $\sum_{j=1}^N \|\mathbf{u}_j^T\|_2^2 = \|\mathbf{U}\|_F^2 = n$ , we obtain

$$\mathbb{E}_P \left[ \mathbb{E}_\epsilon \left[ \|(\mathbf{P}^T \mathbf{U})^T \mathbf{P}^T \epsilon\|_2^2 \right] \right] = \frac{m}{N} \sum_{j=1}^N \sigma_j^2 \|\mathbf{u}_j^T\|_2^2 \leq \frac{m}{N} \|\boldsymbol{\sigma}\|_\infty^2 \sum_{j=1}^N \|\mathbf{u}_j^T\|_2^2 = \frac{mn}{N} \|\boldsymbol{\sigma}\|_\infty^2.$$

Applying Jensen’s inequality, together with eq. (33) yields

$$\mathbb{E}_P [\mathbb{E}_\epsilon [\|U(P^T U)^\dagger P^T \epsilon\|_2]] \leq \frac{N}{(1-\gamma)m} \sqrt{\frac{mn}{N} \|\sigma\|_\infty^2} = \frac{\|\sigma\|_\infty}{(1-\gamma)} \sqrt{\frac{nN}{m}}$$

with probability at least  $1 - \delta$ . Combining (34) with eq. (32) proves the theorem.  $\square$

Theorem 4.6 reveals that as  $m \rightarrow \infty$  (recall we perform uniform sampling with replacement), the upper bound in eq. (29) converges to the usual POD upper bound, i.e.,  $\|\mathbf{f} - \mathbf{U}\mathbf{U}^T \mathbf{f}\|_2$ .

## 5 ODEIM with deterministic sampling

In this section, we present several deterministic strategies that adaptively select sampling points to reduce the quantity  $\|(P^T U)^\dagger\|_2$ , which controls how sensitive the ODEIM oblique projection is to perturbations and noise, cf. Section 2.2. While our probabilistic analysis in Section 4 shows that sampling points that are selected uniformly in  $\{1, \dots, N\}$  are sufficient for ODEIM to be robust with respect to noise, the number of uniformly selected sampling points that are required grows with, e.g., the coherence  $\mu(\mathcal{U})$  of the space  $\mathcal{U}$ . The following deterministic selection strategies aim to achieve robustness with fewer points than uniform sampling by taking information about the space  $\mathcal{U}$  into account.

We first discuss the ODEIM+E sampling algorithm that is based on lower bounds of the smallest eigenvalues of certain structured matrix updates introduced in [30]. We will show that our ODEIM+E approach is a special case of [50], see Section 5.1. Then, we propose an extension of the QDEIM points selection algorithm for selecting oversampling points by interpreting QDEIM as clustering. We call the corresponding procedure ODEIM+C because the oversampling points are selected based on the entropy of clustering information, see Section 5.2. Section 5.3 recaps the classical DEIM algorithm and discusses how it has been extended to select more than  $n$  sampling points, which will serve as our benchmark in the numerical results, and which we call ODEIM+D in the following.

### 5.1 The ODEIM+E sampling algorithm

The goal of the ODEIM+E oversampling algorithm is to select points that minimize  $\|(P^T U)^\dagger\|_2$ . This minimization problem is equivalent to maximizing the smallest singular value of  $P^T U$  because

$$\|(P^T U)^\dagger\|_2 = s_{\max}((P^T U)^\dagger) = \frac{1}{s_{\min}(P^T U)},$$

where  $s_{\max}(\mathbf{M})$  and  $s_{\min}(\mathbf{M})$  denote the largest and smallest singular value of the matrix  $\mathbf{M}$ , respectively. The ODEIM+E algorithm relies on lower bounds on the smallest eigenvalues to select points that maximize  $s_{\min}(P^T U)$  by leveraging the eigenvector corresponding to the smallest eigenvalue, as proposed in [50].

#### 5.1.1 Singular values after symmetric rank-one updates

Consider the basis matrix  $\mathbf{U}$  and the sampling points matrix<sup>1</sup>  $\mathbf{P}_m$  that takes  $m \geq n$  samples. Consider now the SVD of  $\mathbf{P}_m^T \mathbf{U} \in \mathbb{R}^{m \times n}$

$$\mathbf{V}_m \mathbf{\Sigma}_m \mathbf{W}_m^T = \mathbf{P}_m^T \mathbf{U},$$

where  $\mathbf{V}_m \in \mathbb{R}^{m \times n}$  contains, as its columns, the left-singular vectors, the matrix  $\mathbf{\Sigma}_m = \text{diag}[s_1^{(m)}, \dots, s_n^{(m)}] \in \mathbb{R}^{n \times n}$  is a diagonal matrix with the singular values  $s_1^{(m)}, \dots, s_n^{(m)}$ , in descending order, and  $\mathbf{W}_m \in \mathbb{R}^{n \times n}$  contains, as its columns, the right-singular vectors. Note that we assume that  $\mathbf{P}_m^T \mathbf{U}$  has full column rank in

<sup>1</sup>Note that we have changed the notation slightly here and added the subscript “ $m$ ” to  $\mathbf{P}$ . This will help distinguish the sampling points matrix when new indices are added.

the following, which can be ensured by initializing ODEIM+E with, e.g., the QDEIM interpolation points. If we add a sampling point, we obtain

$$\mathbf{P}_{m+1}^T \mathbf{U} = \begin{bmatrix} \mathbf{P}_m^T \mathbf{U} \\ \mathbf{u}_+ \end{bmatrix} \in \mathbb{R}^{m+1 \times n},$$

where  $\mathbf{u}_+ \in \mathbb{R}^{1 \times n}$  is the row of  $\mathbf{U}$  that is selected by the new sampling point. Following the work by Zimmermann et al. [50], the change of the singular values of  $\mathbf{P}_m^T \mathbf{U}$  to  $\mathbf{P}_{m+1}^T \mathbf{U}$  can be understood via a symmetric rank-one update. We have

$$\mathbf{P}_{m+1}^T \mathbf{U} = \begin{bmatrix} \mathbf{V}_m & 0 \\ 0 & 1 \end{bmatrix} \begin{bmatrix} \boldsymbol{\Sigma}_m \\ \mathbf{u}_+ \mathbf{W}_m \end{bmatrix} \mathbf{W}_m^T.$$

The singular values of  $\mathbf{P}_{m+1}^T \mathbf{U}$  are given by the square roots of the eigenvalues of  $(\mathbf{P}_{m+1}^T \mathbf{U})^T (\mathbf{P}_{m+1}^T \mathbf{U})$ , which we represent as

$$(\mathbf{P}_{m+1}^T \mathbf{U})^T (\mathbf{P}_{m+1}^T \mathbf{U}) = \mathbf{W}_m (\boldsymbol{\Sigma}_m^2 + \mathbf{W}_m^T \mathbf{u}_+^T \mathbf{u}_+ \mathbf{W}_m) \mathbf{W}_m^T.$$

With  $\bar{\mathbf{u}}_+ = \mathbf{W}_m^T \mathbf{u}_+^T$ , we obtain  $\Lambda_{m+1} = \boldsymbol{\Sigma}_m^2 + \bar{\mathbf{u}}_+ \bar{\mathbf{u}}_+^T$ , which is a symmetric rank-one update to the diagonal matrix  $\boldsymbol{\Sigma}_m^2$ . The square roots of the eigenvalues of  $\Lambda_{m+1}$  are the singular values of  $\mathbf{P}_{m+1}^T \mathbf{U}$ .

Let  $\lambda_1^{(m)}, \dots, \lambda_n^{(m)}$  be the eigenvalues of  $\boldsymbol{\Sigma}_m^2$  and let  $\lambda_1^{(m+1)}, \dots, \lambda_n^{(m+1)}$  be the eigenvalues of  $\Lambda_{m+1}$ . Our goal is now to select a row of  $\mathbf{U}$  that maximizes the smallest eigenvalue  $\lambda_1^{(m+1)}$ . From Weyl's theorem [44,45] we have that  $\lambda_n^{(m+1)} \geq \lambda_n^{(m)}$ , which shows that adding any sampling point will, at least, not increase  $\|(\mathbf{P}_{m+1}^T \mathbf{U})^\dagger\|_2$  compared to  $\|(\mathbf{P}_m^T \mathbf{U})^\dagger\|_2$ .

### 5.1.2 Lower bounds for eigenvalues of updated matrices

We now use the results by Ipsen et al. in [30] to derive a heuristic strategy with the aim of selecting sampling points that lead to a fast increase of the smallest eigenvalue, i.e., to a fast decrease of  $\|(\mathbf{P}_m^T \mathbf{U})^\dagger\|_2$ .

Let  $g = \lambda_{n-1}^{(m)} - \lambda_n^{(m)}$  be the eigengap. Note that we need  $\lambda_{n-1}^{(m)} > \lambda_n^{(m)}$  in the following. Let  $\mathbf{z}_n^{(m)} \in \mathbb{R}^n$  be the eigenvector of  $\boldsymbol{\Sigma}_m^2$  corresponding to the smallest eigenvalue  $\lambda_n^{(m)}$ , with  $\|\mathbf{z}_n^{(m)}\|_2 = 1$ . In our case  $\mathbf{z}_n^{(m)}$  is the  $n$ -th canonical unit vector of dimension  $n$  because  $\boldsymbol{\Sigma}_m^2$  is diagonal with diagonal elements ordered descending. Then, as shown in [30, Corollary 2.2],

$$\lambda_n^{(m+1)} \geq \lambda_n^{(m)} + \frac{1}{2} \left( g + \|\bar{\mathbf{u}}_+\|_2^2 - \sqrt{(g + \|\bar{\mathbf{u}}_+\|_2^2)^2 - 4g(\mathbf{z}_n^{(m)T} \bar{\mathbf{u}}_+)^2} \right). \quad (34)$$

Observe that the bound eq. (34) depends on the *eigenvector* corresponding to the smallest eigenvalue. We simplify the bound eq. (34) and obtain

$$\lambda_n^{(m+1)} \geq \lambda_n^{(m)} + \frac{g(\mathbf{z}_n^{(m)T} \bar{\mathbf{u}}_+)^2}{g + \|\bar{\mathbf{u}}_+\|_2^2}, \quad (35)$$

which is true because  $1 - \sqrt{1 - b/a^2} \geq b/(2a^2)$  for  $a^2 \geq b \geq 0$ .

### 5.1.3 The ODEIM+E algorithm

The bound eq. (35) motivates us to add the row of  $\mathbf{U}$  that maximizes the Euclidean inner product with the eigenvector  $\mathbf{z}_n^{(m)}$ , i.e., the row that maximizes

$$\mathbf{z}_n^{(m)T} \bar{\mathbf{u}}_+. \quad (36)$$

The criterion eq. (36) is a special case of the criteria developed in [50]. While we build on the perturbation bounds introduced in [30], the authors of [50] directly prove that selecting the point corresponding to the largest absolute inner product with the eigenvector  $\mathbf{z}_n$  is a good choice for a sampling point,

---

**Algorithm 2** Sampling points selection with ODEIM+E

---

```
1: procedure ODEIM+E( $U, m$ )
2:    $n = \text{size}(U, 2)$ 
3:    $\phi = \text{QDEIM}(U, n)$ 
4:   for  $i = n + 1 : m$  do
5:      $[\sim, \mathbf{S}, \mathbf{W}] = \text{SVD}(U[\phi, :], 0)$ 
6:      $\mathbf{r} = (\mathbf{W}[:, \text{end}]^T \mathbf{U}^T) \cdot \sim^2$ 
7:      $[\sim, I] = \text{sort}(\mathbf{r}, \text{'descend'})$ 
8:      $k = 1$ 
9:     while  $\text{any}(I[k] == \phi)$  do
10:       $k = k + 1$ 
11:    end while
12:     $\phi[i] = I[k]$ 
13:  end for
14: return  $\phi$ 
15: end procedure
```

---

see [50, page A2834] and [50, Remark 2, item 3]. In fact, the work [50] goes a step further and also takes into account inner products with eigenvectors corresponding to larger eigenvalues. We do not consider these additional steps discussed in [50] in the following.

The ODEIM+E sampling approach that we consider is summarized in Algorithm 2. It iteratively selects new sampling points in a greedy fashion based on the inner product eq. (36). In line 3 of Algorithm 2, the first  $n$  points are selected with QDEIM, see Algorithm 1. Then, for each oversampling point  $i = n + 1, \dots, m$ , the SVD of  $U[\phi, :]$  is computed to obtain the right-singular vectors. The inner product eq. (36) is computed, where we use that the eigenvector is the  $n$ -th canonical unit vector of dimension  $n$  and so  $\mathbf{z}_n^{(i)T} \bar{\mathbf{u}}_+ = \mathbf{z}_n^{(i)} \mathbf{W}_i^T \mathbf{u}_+^T = \mathbf{W}_i[:, \text{end}]^T \mathbf{u}_+^T$ . Finally, the point with the largest inner product is added, if it has not been selected before. This process is repeated.

Each iteration in ODEIM+E requires performing an SVD of a small matrix whose size grows with the reduced dimension  $n$  and the number of sampling points. Each SVD is in  $\mathcal{O}(n^2 m)$  (for  $m > n$ ). Thus, selecting  $m$  points with ODEIM+E is in  $\mathcal{O}(n^2 m^2)$ . Note that the sampling point selection is performed during the construction of the reduced system in the offline phase.

## 5.2 The ODEIM+C oversampling algorithm based on QDEIM and entropy estimation of clustering information

The QDEIM algorithm is summarized in Algorithm 1. If QDEIM as in Algorithm 1 is used to select more  $m > n$  points than the dimension  $n$  of the DEIM space  $\mathcal{U}$ , for example by applying pivoted QR to the square matrix  $\mathbf{U}\mathbf{U}^T \in \mathbb{R}^{N \times N}$ , then this amounts to choosing the  $m - n$  additional points based on numerical noise because  $\mathbf{U}\mathbf{U}^T$  has only rank  $n$  and the ordering of the columns with index greater than  $n$  has typically no particular mathematical meaning. Instead, we establish a connection between QDEIM and clustering, and use the concept of entropy to select  $m > n$  sampling points in a principled way. We call the corresponding oversampling algorithm ODEIM+C.

### 5.2.1 Sampling points selection and clustering

We now approach the sampling point selection from a different perspective. Consider the nonlinear snapshots matrix  $\mathbf{F} = [\mathbf{f}(\mathbf{x}; \xi_1), \dots, \mathbf{f}(\mathbf{x}; \xi_M)]$ , and interpret each row of  $\mathbf{F}$  as the evolution (trajectory) of a particular spatial position (state) with respect to parameter changes (and with respect to time, in case of time-dependent systems, where  $\xi_i = i\delta t$  is time at time step  $i$  with time step size  $\delta t$ ). We expect that parts

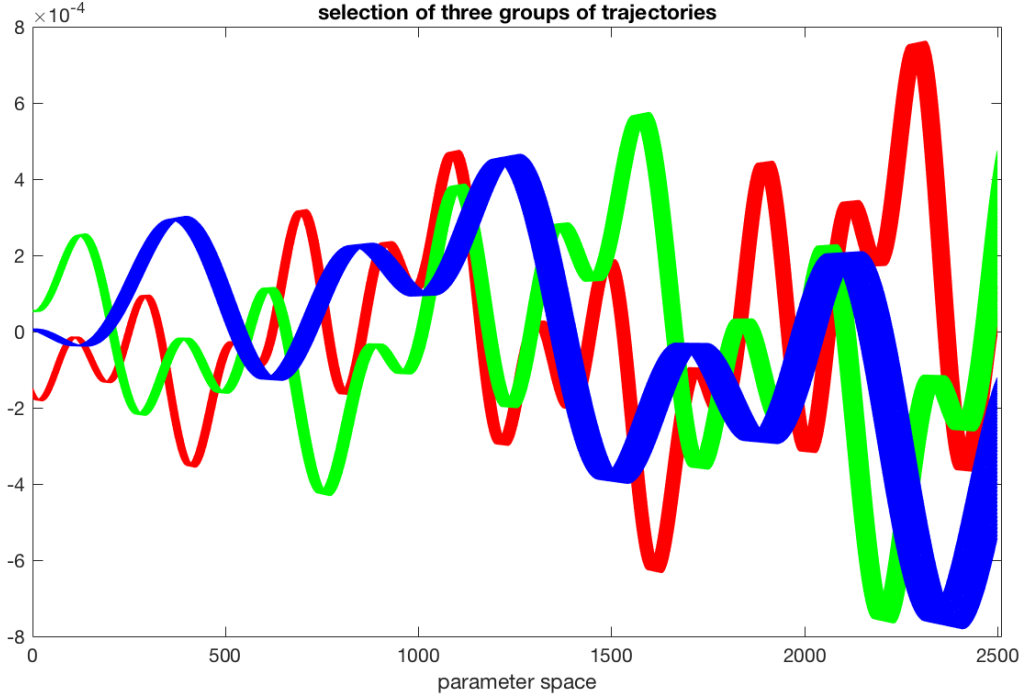


Figure 2: Selected trajectories generated by eq. (7):  $\mathbf{F}[1 : 51, :]$  (red),  $\mathbf{F}[700 : 750, :]$  (green) and  $\mathbf{F}[2200 : 2250, :]$  (blue). Each stripe is a cluster of 51 trajectories and in each cluster the trajectory closest to the mean of the stripe is a reasonably good approximation to all trajectories in the cluster. Note that the widths of the stripes differ, i.e., the clusters are not equally tight.

of the physical domain exhibit similar behavior so that the rows of  $\mathbf{F}$  comprise several clusters.

### 5.2.2 Motivation, discussion, and a numerical example

To illustrate this idea, we use the data generated by eq. (7) in Section 2.2 and plot three groups of neighboring rows of  $\mathbf{F}$ ; see Figure 2. In general, neighboring row indices in  $\mathbf{F}$  do not necessarily mean neighboring positions in the spatial domain, as various mappings are used to map the spatial domain coordinates into a suitable data structure during discretization. It is a clustering method that will partition the row indices to define a suitable clustering. The graphs in Figure 2 clearly show three groups (clusters).

Let  $\mathbf{U}\mathbf{\Sigma}\mathbf{W}^T$  be the truncated SVD of the snapshot matrix  $\mathbf{F}$ , with the DEIM basis matrix  $\mathbf{U} \in \mathbb{R}^{N \times n}$ , the diagonal matrix  $\mathbf{\Sigma} \in \mathbb{R}^{n \times n}$ , and the matrix of the right-singular vectors  $\mathbf{W} \in \mathbb{R}^{M \times n}$ . We can interpret each row of  $\mathbf{U}\mathbf{\Sigma}$  (and of  $\mathbf{U}$ ) as coordinates of the corresponding row of  $\mathbf{F}$  that is represented in the basis  $\mathbf{W}^T$  (and  $\mathbf{\Sigma}\mathbf{W}^T$ , respectively). Thus, selecting row indices of  $\mathbf{U}$  for DEIM can be recast into finding clusters of the trajectories. We now will briefly review k-means clustering to establish that QDEIM can be interpreted as a clustering method.

### 5.2.3 Clustering with k-means

Denote the columns of  $\mathbf{F}^T$  as  $\mathbf{a}_1, \dots, \mathbf{a}_N$  and define the set  $\mathcal{A} = \{\mathbf{a}_1, \dots, \mathbf{a}_N\} \subset \mathbb{R}^M$ . Let further  $\pi = [\pi_1, \dots, \pi_n]$  be a partition of the index set  $\{1, \dots, N\}$ , which means that  $\bigcup_{i=1}^n \pi_i = \{1, \dots, N\}$  and  $\pi_i \cap \pi_j = \emptyset$

for  $i \neq j$ . Let  $\#\pi_i$  denote the cardinality of  $\pi_i$  for  $i = 1, \dots, n$ . Recall, the k-means algorithm clusters  $N$  points in  $\mathbb{R}^M$  into  $n$  clusters with respect to the Euclidean metrics by minimizing the objective function

$$\mathfrak{F}(\pi) = \sum_{i=1}^n \sum_{j \in \pi_i} \|\mathbf{a}_j - \mathbf{c}_i\|_2^2, \quad \text{where} \quad \mathbf{c}_i = \frac{1}{\#\pi_i} \sum_{j \in \pi_i} \mathbf{a}_j, \quad (37)$$

see, e.g., [28] for an introduction to k-means clustering. The k-means aims to minimize eq. (37) iteratively. The iterations start with an initial partition  $\pi^{(0)}$ , with the corresponding set of centroids  $\mathbf{c}_i^{(0)}$ ; at each iteration  $k$  the centroids  $\mathbf{c}_i^{(k)}$ ,  $i = 1, \dots, n$ , induce a new partitioning  $\pi^{(k+1)} = [\pi_1^{(k+1)}, \dots, \pi_n^{(k+1)}]$ , with the corresponding centroids by

$$\pi_i^{(k+1)} = \left\{ j : \|\mathbf{a}_j - \mathbf{c}_i^{(k)}\|_2 \leq \min_{\ell} \|\mathbf{a}_j - \mathbf{c}_\ell^{(k)}\|_2 \right\}, \quad \mathbf{c}_i^{(k+1)} = \frac{1}{\#\pi_i^{(k+1)}} \sum_{j \in \pi_i^{(k+1)}} \mathbf{a}_j. \quad (38)$$

As a result,  $\mathfrak{F}(\pi^{(k+1)}) \leq \mathfrak{F}(\pi^{(k)})$ . This is repeated until at some index  $k$  the change of  $\mathfrak{F}(\pi^{(k)})$  drops below a given threshold. Note that  $\mathfrak{F}(\pi^{(k)})$  converges as  $k \rightarrow \infty$ .

#### 5.2.4 Relaxed k-means

Clustering with k-means searches for an optimum of a nonconvex objective and therefore the outcome of k-means typically depends on the initialization and the optimization even can get stuck in local optima. Several approaches have been proposed to make optimization underlying k-means more robust. We are particularly interested in relaxing the discrete condition in the objective function eq. (37) as it has been done in [47].

The partition  $\pi = [\pi_1, \dots, \pi_n]$  can be encoded in a matrix  $\mathbf{C}$  as follows: for all  $1 \leq i \leq N$ ,  $1 \leq j \leq n$ , set  $C_{ij} = 1/\sqrt{\#\pi_j}$  if the  $i$ th point belongs to the  $j$ th cluster, and to zero otherwise. Then, minimizing the objective of k-means clustering  $\mathfrak{F}(\pi)$  over the partitions  $\pi$  is equivalent to minimizing  $\mathfrak{F}(\mathbf{C})$  over the set  $\mathcal{P}_n(N)$  of partitioning matrices  $\mathbf{C}$ . The objective can be rewritten as  $\mathfrak{F}(\mathbf{C}) = \text{trace}(\mathbf{F}\mathbf{F}^T) - \text{trace}(\mathbf{C}^T \mathbf{F}\mathbf{F}^T \mathbf{C})$ , and, thus, the minimization of eq. (37) over all partitions  $\pi$  is equivalent to solving

$$\max_{\mathbf{C} \in \mathcal{P}_n(N)} \text{trace}(\mathbf{C}^T \mathbf{F}\mathbf{F}^T \mathbf{C}). \quad (39)$$

Following [47], the NP-hard combinatorial optimization eq. (39) is relaxed by allowing  $\mathbf{C}$  from the Stiefel manifold  $\mathcal{V}_n(\mathbb{R}^N)$  of  $N \times n$  orthonormal matrices, i.e., the continuous optimization of the trace of the Rayleigh quotient is obtained

$$\max_{\mathbf{\Omega} \in \mathcal{V}_n(\mathbb{R}^N)} \text{trace}(\mathbf{\Omega}^T \mathbf{F}\mathbf{F}^T \mathbf{\Omega}). \quad (40)$$

By the Ky Fan theorem [47, page 3], the optimal solutions of eq. (40) are given by  $\mathbf{\Omega} = \mathbf{U}\mathbf{Q}$ , where  $\mathbf{U} = [\mathbf{u}_1, \dots, \mathbf{u}_n]$  is the matrix of the eigenvectors belonging to the  $n$  largest eigenvalues of  $\mathbf{F}\mathbf{F}^T$  and  $\mathbf{Q}$  is any  $n \times n$  orthogonal matrix. Clearly, the columns of  $\mathbf{U}$  are the DEIM basis vectors, i.e., the left singular vectors of the largest singular values  $s_1(\mathbf{F}) \geq \dots \geq s_n(\mathbf{F})$  of  $\mathbf{F}$ . For the sake of technical simplicity we assume that  $s_n(\mathbf{F}) > s_{n+1}(\mathbf{F})$  in the following.

It remains to use the freedom in choosing  $\mathbf{Q}$  to determine a continuous solution  $\mathbf{\Omega}$  that is close to a discrete matrix that yields a nearly optimal partition (clustering). Recall that QDEIM is invariant under orthonormal change of basis, i.e., it computes the same index selection for any  $\mathbf{\Omega} = \mathbf{U}\mathbf{Q}$ , independent of a particular choice of  $\mathbf{Q}$ .

#### 5.2.5 Connection of relaxed k-means clustering to QDEIM

Let us now show that QDEIM gives a discretization of one particular continuous solution  $\mathbf{\Omega}_* \in \mathcal{V}_n(\mathbb{R}^N)$  of the relaxed k-means problem eq. (40).



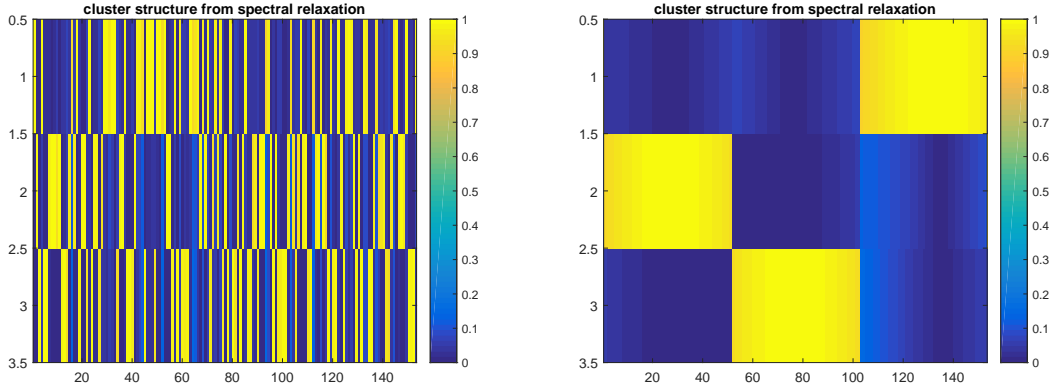


Figure 3: Clustering by spectral relaxation of the trajectories shown in Figure 2, stacked in a block of data as  $\mathbf{X} = (\mathbf{F}(1 : 51, :)^T, \mathbf{F}(700 : 750, :)^T, \mathbf{F}(2200 : 2250, :)^T)\Pi$ , where  $\Pi$  is a random permutation matrix. The figure in the first panel is produced by `imagesc(abs( $\tilde{\mathbf{R}}$ ))`. The second panel is obtained from the first by inverting  $\Pi$  to confirm correct clustering.

POD-QDEIM and POD-KDEIM, where KDEIM refers to finding the sampling points via k-means clustering as discussed in Section 5.2.5; see, Algorithm 3. The relative reconstruction errors for the quantity of the interest  $y(t)$  are  $\epsilon_{\text{QDEIM}} = 0.783045 \times 10^{-5}$  and  $\epsilon_{\text{KDEIM}} = 2.388807 \times 10^{-4}$ , illustrating accurate approximations by both models. Figure 4 shows the output for the full model and both reduced models. As our discussion suggests, for this example, the two approaches are comparable.

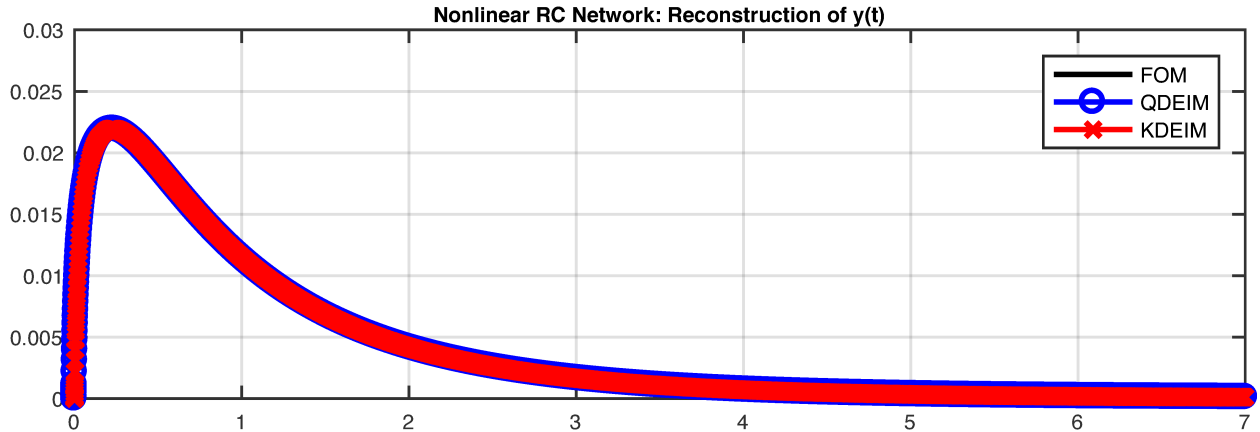


Figure 4: (Nonlinear RC Circuit) The reconstruction accuracy of  $y(t)$  by QDEIM and KDEIM.

### 5.2.7 Sample selection based on entropy and clustering information

The QDEIM points selection algorithm selects the indices corresponding to the first  $n$  columns of  $\tilde{\mathbf{R}}$ , see Algorithm 1. We now introduce ODEIM+C that uses the interpretation of QDEIM as clustering to select  $m > n$  points.

The absolute values of the components of each column in  $\tilde{\mathbf{R}}$  indicate how well the columns are aligned with

---

**Algorithm 3** Implementation of KDEIM

---

```
1: procedure KDEIM( $\mathbf{U}$ )
2:    $[\sim, n] = \text{size}(\mathbf{U})$ 
3:    $\phi = \text{zeros}(n, 1)$ 
4:    $[I, \mathbf{C}] = \text{kmeans}(\mathbf{U}, n)$  ▷ use the default Euclidean metric
5:   for  $i = 1, \dots, n$  do
6:      $J = \text{find}(I == i)$  ▷ select the  $i$ -th cluster
7:      $\mathbf{Z} = \mathbf{U}[J, :] - \text{ones}(\text{length}(J), 1)\mathbf{C}[i, :]$ 
8:      $[\sim, \ell] = \text{min}(\text{sum}(\mathbf{Z} * \mathbf{Z}, 2) ./ \text{sum}(\mathbf{U}[J, :].^2, 2))$ 
9:      $\phi[i] = J[\ell[1]]$  ▷ cluster representative closest to centroid
10:  end for
11: return  $\phi$ 
12: end procedure
```

---

the corresponding basis vector given by  $\mathbf{R}_1$ . If a column is well aligned with one of the basis vectors, then there is one component that significantly dominates all other components in that column with respect to its absolute values. In contrast, if the column is not well aligned with any of the basis vectors, then none of the components of the column dominates. Typically, in the first case, i.e., the column is well aligned with a basis vector, the column has a low entropy, whereas in the second case, i.e., the column is not well aligned with any basis vector, the column has a higher entropy. Algorithm 4 computes the entropy of each column and selects the sampling points corresponding to the columns with the highest entropy, i.e., that are heuristically least aligned with any of the basis vectors. First, the QR factorization of  $\mathbf{U}^T$  is computed. Then,  $\tilde{\mathbf{R}}$  is formed and its columns are normalized. The entropy of each column of the normalized  $\tilde{\mathbf{R}}$  is computed based on the natural logarithm as  $e(\tilde{\mathbf{R}}[:, i]) = -\tilde{\mathbf{R}}[:, i]^T \log(\tilde{\mathbf{R}}[:, i])$ . Note that we use the convention  $0 \log(0) = 0$  in the computation of the entropy  $e(\tilde{\mathbf{R}}[:, i])$ . The components of the entropy vector  $\mathbf{e} = [e(\tilde{\mathbf{R}}[:, 1]), \dots, e(\tilde{\mathbf{R}}[:, N])]$  are sorted descending and the sampling points corresponding to the first  $m - n$  components are used.

### 5.3 The ODEIM+D oversampling algorithm based on classical DEIM points selection

Algorithm 5 summarizes the classical DEIM points selection algorithm, which selects interpolation points based on the residual of the DEIM approximation. The version presented in Algorithm 5 iterates from  $1, \dots, m$ , instead of  $1, \dots, n$ , to select  $m > n$  sampling points. Note that similar extension to selecting  $m > n$  points with the DEIM algorithm have been introduced in, e.g., [14–16, 48].

## 6 Numerical results

This section demonstrates ODEIM with randomized and deterministic oversampling algorithms on numerical examples. Section 6.1 revisits the toy example from Section 2.2 and demonstrates that ODEIM provides a stable approximation compared to DEIM. Section 6.2 demonstrates ODEIM on a diffusion-reaction problem, where ODEIM provides stable approximations in contrast to DEIM.

### 6.1 Synthetic example

Let us revisit the synthetic example introduced in Section 2.2. We use the same setup as before but now approximate the noisy function with ODEIM based on deterministic oversampling algorithms introduced in Section 5 and randomized oversampling. The randomized oversampling ODEIM+rand selects the first  $n$  sampling points with QDEIM and the  $m - n$  oversampling points uniformly *without replacement* from the set of indices  $\{1, \dots, N\}$ . The number of sampling points is set to  $m = 2n$  in case of oversampling. We perform 10 replicates of the experiments, compute the  $L_2$  error as defined in eq. (8), and then average the

---

**Algorithm 4** Oversampling with ODEIM+C

---

```
1: procedure ODEIM+C( $U, m$ )
2:    $[\sim, \mathbf{R}, \mathbf{p}] = \text{qr}(\mathbf{U}^T, \text{'vector'})$ 
3:    $[N, n] = \text{size}(U)$ 
4:    $\phi = \mathbf{p}[1 : n]$ 
5:    $\tilde{\mathbf{R}} = \mathbf{R}[1 : n, 1 : n] \setminus \mathbf{R}$ 
6:    $s = \text{sum}(\text{abs}(\tilde{\mathbf{R}}), 1)$ 
7:    $\tilde{\mathbf{R}} = \text{abs}(\tilde{\mathbf{R}}) ./ \text{repmat}(s, \text{size}(\tilde{\mathbf{R}}, 1), 1)$  ▷ take absolute value and normalize
8:    $e = \text{zeros}(N, 1)$ 
9:   for  $i = 1 : N$  do
10:     $I = \tilde{\mathbf{R}}[:, i] > 0;$ 
11:     $e[i] = -\tilde{\mathbf{R}}[I, i]^T \log(\tilde{\mathbf{R}}[I, i])$ 
12:  end for
13:   $[\sim, I] = \text{sort}(e, \text{'descend'})$ 
14:   $i = 1$ 
15:  while  $\text{length}(\phi) < m$  do
16:     $\phi = \text{unique}([\phi, \mathbf{p}(I(i))])$ 
17:     $i = i + 1$ 
18:  end while
19: return  $\phi$ 
20: end procedure
```

---

$L_2$  errors over the 10 replicates, see Figure 5. The results indicate that oversampling avoids the unstable behavior obtained with DEIM, cf. Figure 1. All oversampling algorithms perform well in this example, with ODEIM+E achieving the lowest errors.

## 6.2 Diffusion problem with nonlinear reaction term

We now demonstrate ODEIM with a reduced model of a diffusion-reaction problem. The example demonstrates that instabilities in the DEIM approximation can lead to unstable reduced models, which can be avoided with ODEIM.

### 6.2.1 Problem setup

Let  $\Omega = (0, 1)^2 \subset \mathbb{R}^2$  and consider the PDE

$$\Delta u(\mathbf{x}; \boldsymbol{\xi}) + f(u(\mathbf{x}; \boldsymbol{\xi}); \boldsymbol{\xi}) = 100 \sin(2\pi x_1) \sin(2\pi x_2), \quad \mathbf{x} \in \Omega, \quad (42)$$

where  $\mathbf{x} = [x_1, x_2]^T$  is the spatial coordinate,  $u : \Omega \times \mathcal{D} \rightarrow \mathbb{R}$  is the solution function, and  $f : \mathbb{R} \times \mathcal{D} \rightarrow \mathbb{R}$  is a nonlinear function

$$f(u; \boldsymbol{\xi}) = (0.1 \sin(\xi_1) + 2) \exp(-2.7\xi_1^2) (\exp(\xi_2 u 1.8) - 1),$$

with parameter  $\boldsymbol{\xi} = [\xi_1, \xi_2]^T \in \mathcal{D}$ . The PDE eq. (42) is closed with homogeneous Dirichlet boundary conditions. This example is a modification of the example considered in [27].

We discretize eq. (42) with finite difference on an equidistant mesh with mesh width  $h = 1/256$  in  $\Omega$ . The system of nonlinear equations is solved with Newton's method and inexact line search based on the Armijo condition. The output of the discretized full model is the vector of evaluations of the discrete approximation of  $u$  at the points  $[0.25i, 0.2j]^T \in \Omega$  with  $i = 1, 2, 3$  and  $j = 1, 2, 3, 4$ . We derive a reduced model from 1600 snapshots corresponding to an equidistant grid of parameter values in the domain  $\mathcal{D} = [-\pi/2, \pi/2]^2$ . The basis is constructed with POD. The POD dimension is chosen as  $r = 50$ . The nonlinear term is approximated with empirical interpolation, where the nonlinear function evaluations  $f$  are perturbed with zero-mean Gaussian noise and standard deviation  $\sigma > 0$ .

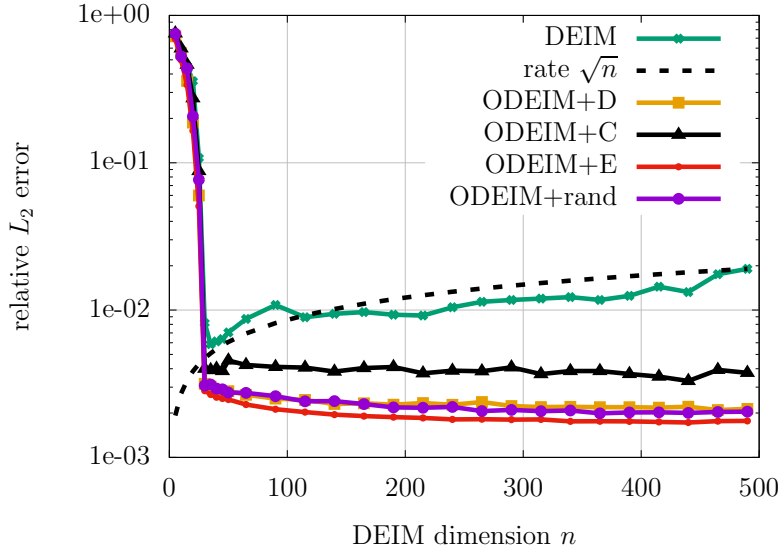


Figure 5: Synthetic example: ODEIM stabilizes DEIM and avoids amplification of noise if sufficiently many oversampling points are selected. Oversampling with ODEIM+E yields the smallest error in this example. All oversampling algorithms stabilize the DEIM approximation in this example.

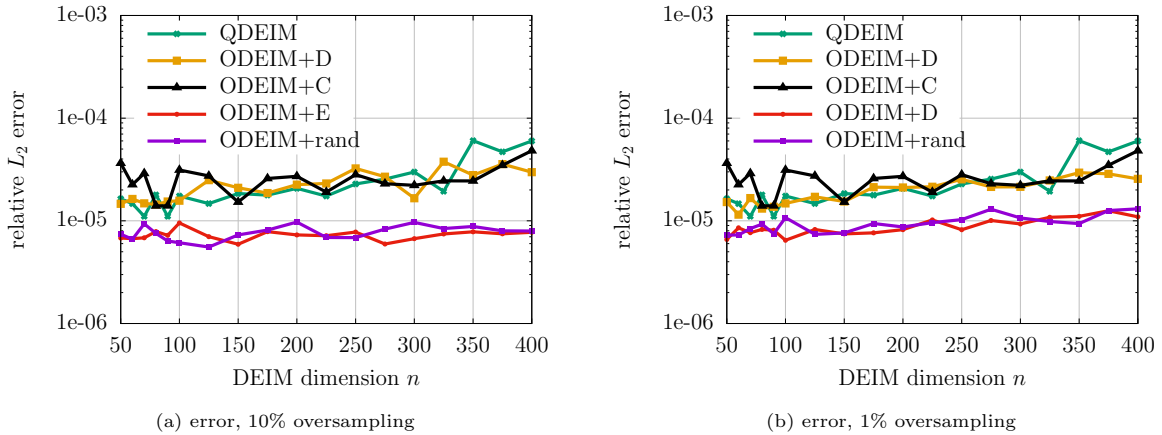


Figure 6: Diffusion reaction example: Approximating the nonlinear term with ODEIM achieves stable behavior in contrast to DEIM approximations where the error grows with the DEIM dimension, see the  $L_2$  errors plotted in (a) and (b). The ODEIM+E and randomized oversampling ODEIM+rand show stable behavior in this example. Standard deviation of noise is  $\sigma = 10^{-3}$ .

---

**Algorithm 5** Oversampling with ODEIM+D
 

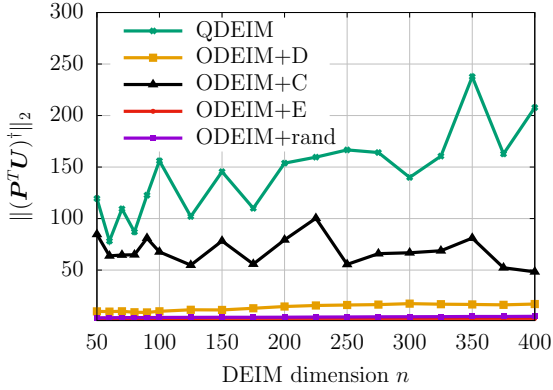
---

```

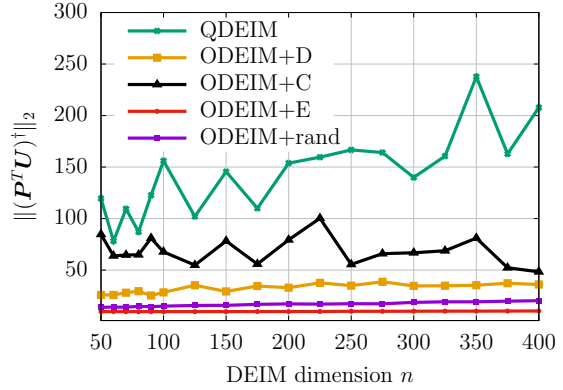
1: procedure ODEIMD( $\mathbf{U}$ ,  $m$ )
2:    $\phi = []$ 
3:    $\mathbf{r} = \mathbf{U}[:, 1]$ 
4:   for  $i = 1 : m$  do
5:      $[\tilde{\cdot}, I] = \max(\text{abs}(\mathbf{r}))$ 
6:      $\phi(i) = I(1)$ 
7:      $d = \min([i, n])$ 
8:      $k = \text{mod}(i, n) + 1$ 
9:      $\mathbf{c} = \mathbf{U}[\phi, 1 : d] \setminus \mathbf{U}[\phi, k]$ 
10:     $\mathbf{r} = \mathbf{U}[:, k] - \mathbf{U}[:, 1 : d]\mathbf{c}$ 
11:   end for
12: return  $\phi$ 
13: end procedure

```

---



(a) norm of sampling operator, 10% oversampling



(b) norm of sampling operator, 1% oversampling

 Figure 7: Diffusion reaction example: Oversampling with ODEIM+E achieves stable behavior in contrast to DEIM approximations in this example, which is reflected in plots (a) and (b) that show that the norm  $\|(\mathbf{P}^T \mathbf{U})^\dagger\|_2$  is lowest in case of ODEIM+E. Standard deviation of noise is  $\sigma = 10^{-3}$ .

## 6.2.2 Results

We compare the errors of various reduced models, which differ in the way the nonlinear term is approximated. With “QDEIM” and “DEIM” we denote in the following reduced models that approximate the nonlinear with QDEIM and DEIM, respectively, without oversampling. Reduced models denoted with “ODEIM+D”, “ODEIM+C”, and “ODEIM+E” approximate the nonlinear terms with the respective oversampling strategies presented in Section 5. The reduced models denoted with “ODEIM+rand” select the first  $n$  points with QDEIM and the subsequent  $m - n$  points randomly with a uniform distribution in  $\{1, \dots, N\}$  without replacement.

Figure 6 compares different reduced systems, where the noise with  $\sigma = 10^{-3}$  is added to the nonlinear function evaluations. We consider the  $L_2$  error over the outputs of the models, where we perform 10 replicates and report the averaged error. Note that the reported errors are with respect to the outputs of the reduced model, rather than the errors of the DEIM approximations, which demonstrates that instabilities in DEIM approximations can significantly impact the output errors of reduced models. Figure 6a uses 10% of the total of  $N$  components as sampling points, which means  $m - n = 6553$  in our example. First, observe that without oversampling the error increases with the dimension of the DEIM space. It seems that neither the ODEIM+D

nor ODEIM+C stabilizes the reduced model in this example. It seems that ODEIM+C selects points that are outliers in the sense of the cluster terminology introduced in Section 5.2. This means that these outlier points correspond to a high entropy as described in Section 5.2 while being unrepresentative for most of the points. This could be explained, in parts, by the static nature of the clustering-based oversampling strategy. The approach is static in the sense that the oversampling points are selected all at once from the decomposition eq. (41) unlike, for example, in the ODEIM+E approach where oversampling points are added one at a time after an update of the involved quantities. In ODEIM+C, it is possible that some columns of  $\mathbf{R}$  with high entropy are nearly linearly dependent; thus they should indeed contribute only one sampling point. With this in mind, one can modify ODEIM+C to make it a dynamic selection approach as well. For example, after adding the highest entropy entry, one can eliminate the columns (even those with high entropies) if they are close to being linearly independent with the current selection. This issue together with other extensions, e.g., incorporating kernel k-means [42] and hierarchical clustering [28] into the DEIM selection process, will be investigated in a separate work; we will not pursue these directions here. The results also indicate that, unlike ODEIM+C and ODEIM+D approaches, ODEIM+E, once again, stabilizes the problem in the sense that the error stays constant for increasing dimensions. Additionally, the random selection strategy ODEIM+rand stabilizes the reduced model too. Similar results are shown in Figure 6b for 1% oversampling points. The norm of the norm  $\|(\mathbf{P}^T \mathbf{U})^\dagger\|_2$  is reported in Figure 7. The norm  $\|(\mathbf{P}^T \mathbf{U})^\dagger\|_2$  grows with the dimension in DEIM and stays nearly constant for ODEIM+E and ODEIM+rand.

Detailed studies of the performance of the four sampling strategies are shown in Figure 8, Figure 9, Figure 10, and Figure 11. The error bars indicate the maximal and minimal error over the 10 replicates. As Figure 6 indicates, oversampling with ODEIM+E and ODEIM+rand seems most effective in this example.

## 7 Conclusions

Empirical interpolation is often used for approximating nonlinear terms in reduced models; however, stability issues have been observed in a wide range of applications. Our probabilistic analysis shows that the particular instability arising due to perturbations, and noisy samples of the nonlinear terms can be avoided by oversampling DEIM. Numerical results demonstrated that instabilities in DEIM can lead to a loss of accuracy in the reduced model outputs and that randomized and deterministic oversampling strategies stabilized DEIM, and thus the reduced model.

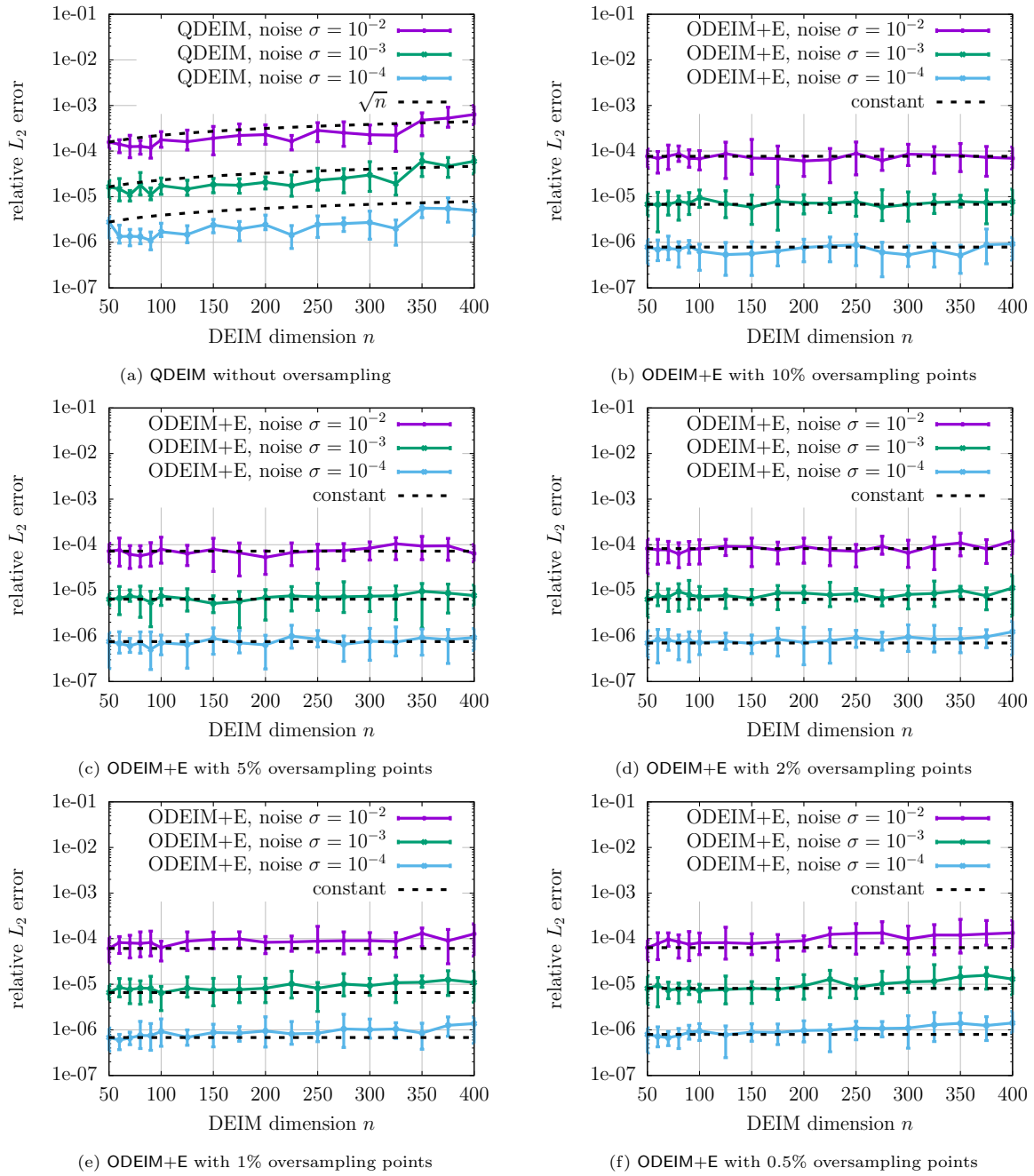
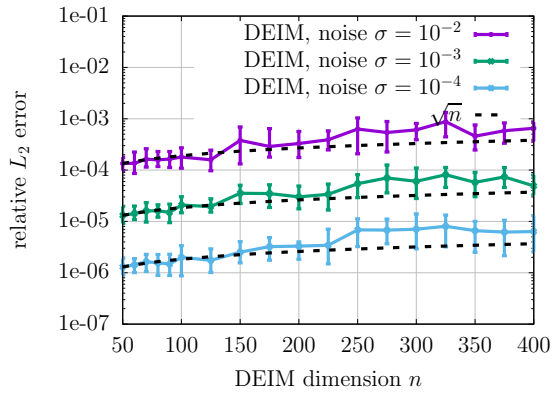
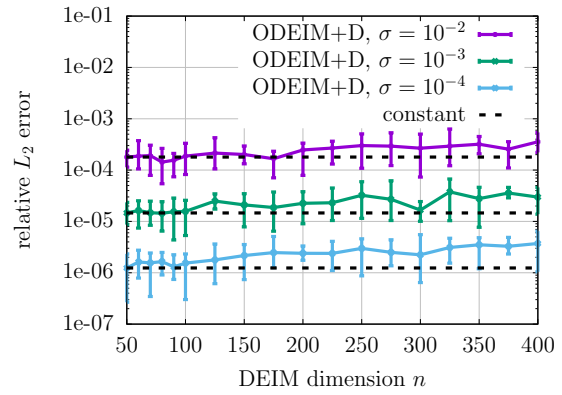


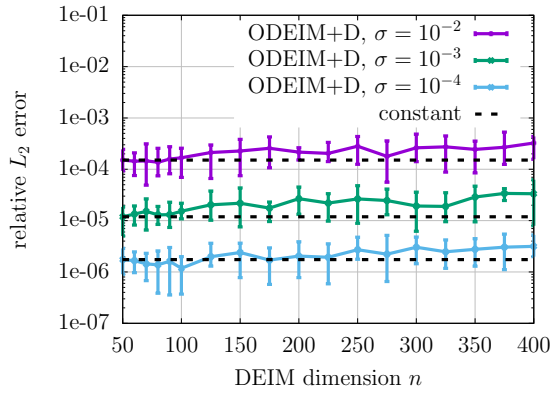
Figure 8: Diffusion reaction example: Oversampling DEIM with ODEIM+E.



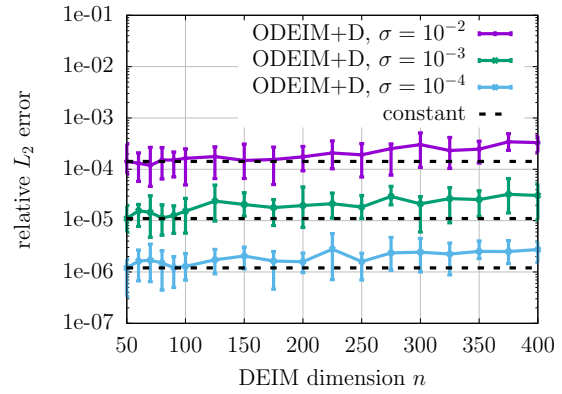
(a) DEIM without oversampling



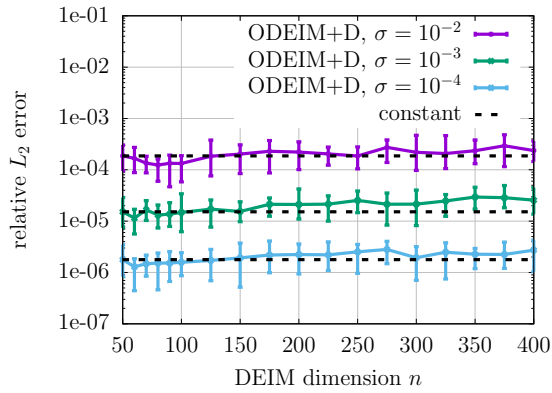
(b) ODEIM+D with 10% oversampling points



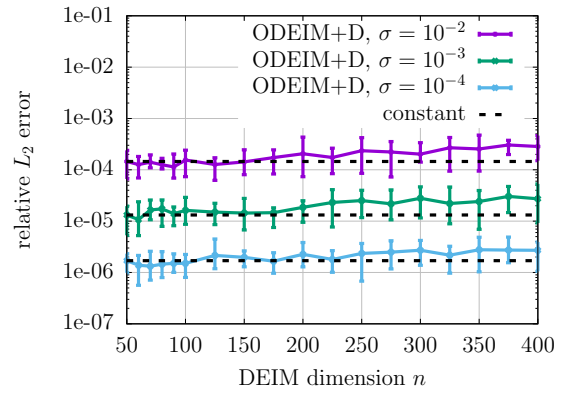
(c) ODEIM+D with 5% oversampling points



(d) ODEIM+D with 2% oversampling points



(e) ODEIM+D with 1% oversampling points



(f) ODEIM+D with 0.5% oversampling points

Figure 9: Diffusion reaction example: Oversampling DEIM with ODEIM+D.

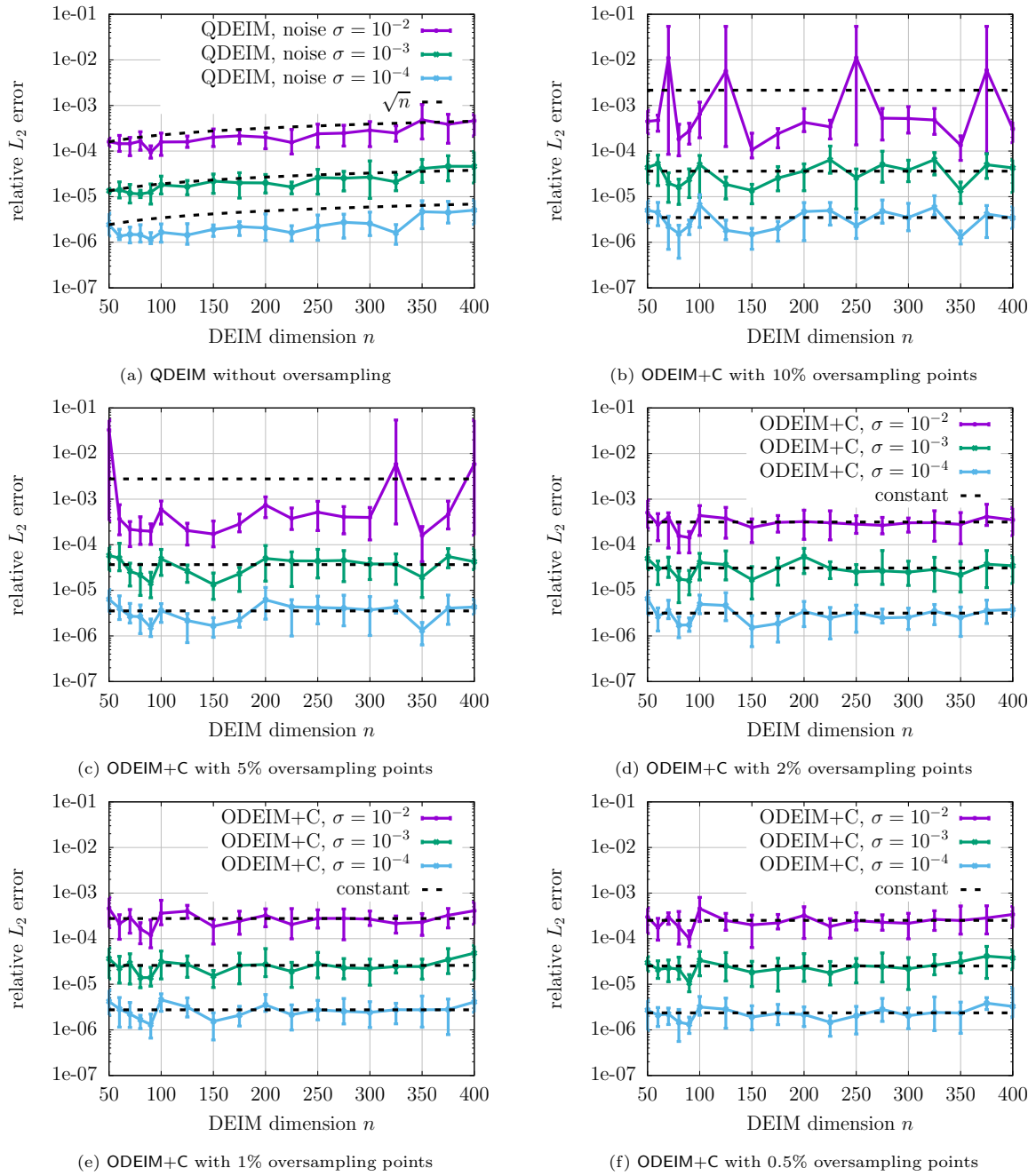


Figure 10: Diffusion reaction example: Oversampling DEIM with ODEIM+C.

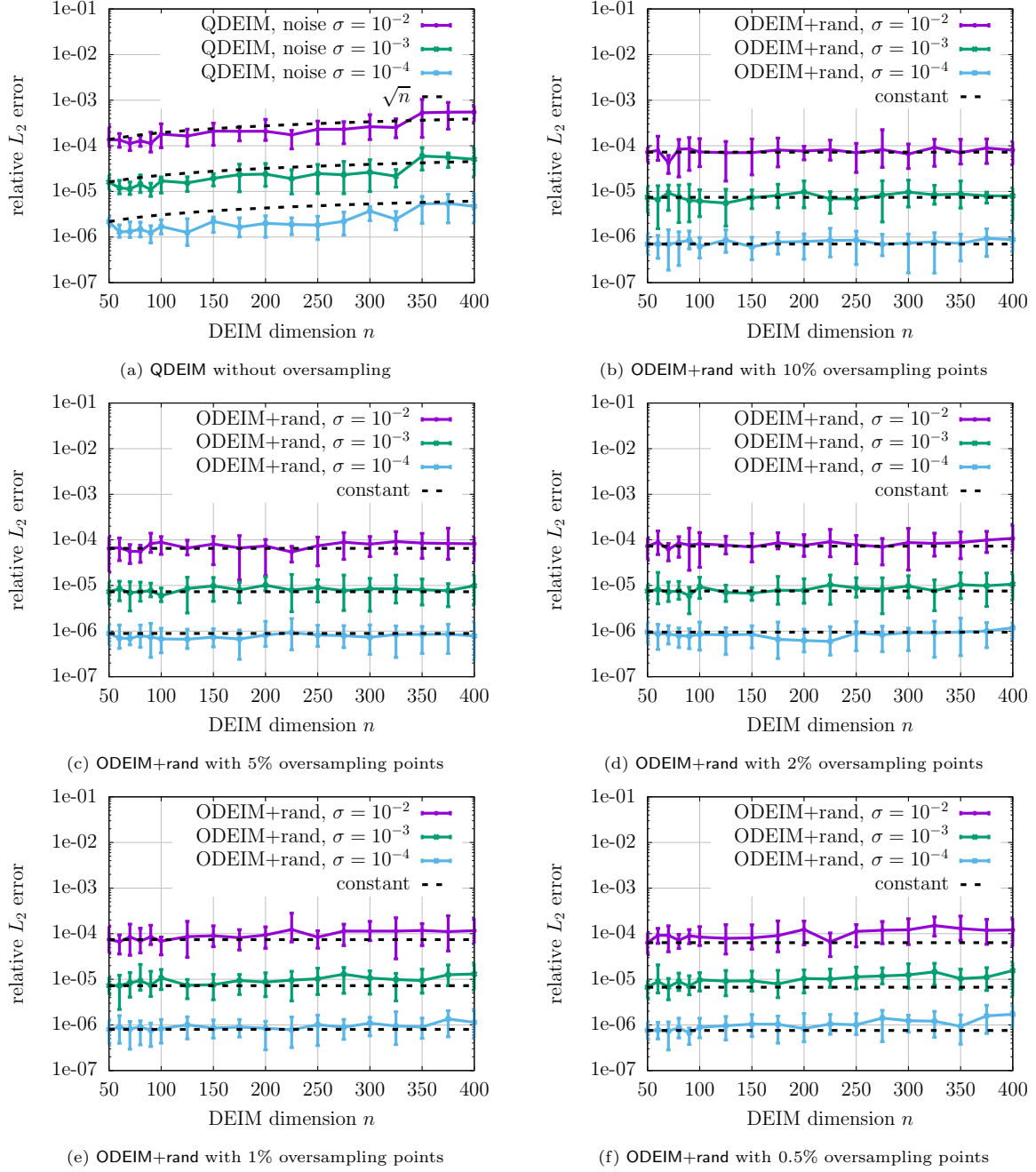


Figure 11: Diffusion reaction example: Oversampling DEIM with oversampling points selected uniformly without replacement from the set of all points. The first  $n$  points are selected with QDEIM.

## References

- [1] J.-P. ARGAUD, B. BOURIQUET, F. DE CASO, H. GONG, Y. MADAY, AND O. MULA, *Sensor placement in nuclear reactors based on the generalized empirical interpolation method*, Journal of Computational Physics, 363 (2018), pp. 354 – 370.
- [2] J. P. ARGAUD, B. BOURIQUET, H. GONG, Y. MADAY, AND O. MULA, *Stabilization of (G)EIM in presence of measurement noise: Application to nuclear reactor physics*, in Spectral and High Order Methods for Partial Differential Equations ICOSAHOM 2016, M. L. Bittencourt, N. A. Dumont, and J. S. Hesthaven, eds., Cham, 2017, Springer International Publishing, pp. 133–145.
- [3] P. ASTRID, S. WEILAND, K. WILLCOX, AND T. BACKX, *Missing point estimation in models described by proper orthogonal decomposition*, in Decision and Control, 2004. CDC. 43rd IEEE Conference on, vol. 2, Dec 2004, pp. 1767–1772 Vol.2.
- [4] P. ASTRID, S. WEILAND, K. WILLCOX, AND T. BACKX, *Missing point estimation in models described by proper orthogonal decomposition*, IEEE Transactions on Automatic Control, 53 (2008), pp. 2237–2251.
- [5] Z. BAI AND D. SKOOGH, *A projection method for model reduction of bilinear dynamical systems*, Linear Algebra and its Applications, 415 (2006), pp. 406–425.
- [6] L. BALZANO, B. RECHT, AND R. NOWAK, *High-dimensional matched subspace detection when data are missing*, in 2010 IEEE International Symposium on Information Theory, June 2010, pp. 1638–1642.
- [7] M. BARRAULT, N. C. NGUYEN, Y. MADAY, AND A. T. PATERA, *An empirical interpolation method: Application to efficient reduced-basis discretization of partial differential equations*, C. R. Acad. Sci. Paris, Série I., 339 (2004), pp. 667–672.
- [8] P. BENNER AND T. BREITEN, *Two-sided projection methods for nonlinear model order reduction*, SIAM Journal on Scientific Computing, 37 (2015), pp. B239–B260.
- [9] P. BENNER, S. GUGERCIN, AND K. WILLCOX, *A survey of projection-based model reduction methods for parametric dynamical systems*, SIAM Review, 57 (2015), pp. 483–531.
- [10] P. BINEV, A. COHEN, O. MULA, AND J. NICHOLS, *Greedy algorithms for optimal measurements selection in state estimation using reduced models*, SIAM/ASA Journal on Uncertainty Quantification, 6 (2018), pp. 1101–1126.
- [11] L. BOS, S. DE MARCHI, A. SOMMARIVA, AND M. VIANELLO, *Computing multivariate Fekete and Leja points by numerical linear algebra*, SIAM Journal on Numerical Analysis, 48 (2010), pp. 1984–1999.
- [12] P. A. BUSINGER AND G. H. GOLUB, *Linear least squares solutions by Householder transformations*, Numerische Mathematik, 7 (1965), pp. 269–276.
- [13] E. J. CANDÈS AND B. RECHT, *Exact matrix completion via convex optimization*, Foundations of Computational Mathematics, 9 (2009), p. 717.
- [14] K. CARLBERG, *Model reduction of nonlinear mechanical systems via optimal projection and tensor approximation*, PhD thesis, Stanford University, 2011.
- [15] K. CARLBERG, C. BOU-MOSLEH, AND C. FARHAT, *Efficient non-linear model reduction via a least-squares Petrov–Galerkin projection and compressive tensor approximations*, International Journal for Numerical Methods in Engineering, 86 (2011), pp. 155–181.
- [16] K. CARLBERG, C. FARHAT, J. CORTIAL, AND D. AMSALLEM, *The GNAT method for nonlinear model reduction: Effective implementation and application to computational fluid dynamics and turbulent flows*, Journal of Computational Physics, 242 (2013), pp. 623–647.

- [17] S. CHATURANTABUT AND D. SORENSEN, *Nonlinear model reduction via discrete empirical interpolation*, SIAM Journal on Scientific Computing, 32 (2010), pp. 2737–2764.
- [18] Y. CHEN, *Model order reduction for nonlinear systems*, Master’s thesis, Massachusetts Institute of Technology, 1999.
- [19] CHKIFA, ABDELLAH, COHEN, ALBERT, MIGLIORATI, GIOVANNI, NOBILE, FABIO, AND TEMPONE, RAUL, *Discrete least squares polynomial approximation with random evaluations - application to parametric and stochastic elliptic PDEs*, ESAIM: M2AN, 49 (2015), pp. 815–837.
- [20] A. COHEN, M. A. DAVENPORT, AND D. LEVIATAN, *On the stability and accuracy of least squares approximations*, Foundations of Computational Mathematics, 13 (2013), pp. 819–834.
- [21] A. DAMLE, V. MINDEN, AND L. YING, *Robust and efficient multi-way spectral clustering*, arXiv preprint arXiv:1609.08251, (2016).
- [22] Z. DRMAČ AND S. GUGERCIN, *A new selection operator for the Discrete Empirical Interpolation Method – improved a priori error bound and extensions*, SIAM Journal on Scientific Computing, 38 (2016), pp. A631–A648.
- [23] Z. DRMAČ AND A. SAIBABA, *The discrete empirical interpolation method: Canonical structure and formulation in weighted inner product spaces*, SIAM Journal on Matrix Analysis and Applications, 39 (2018), pp. 1152–1180.
- [24] J. L. EFTANG AND B. STAMM, *Parameter multi-domain ‘hp’ empirical interpolation*, International Journal for Numerical Methods in Engineering, 90 (2012), pp. 412–428.
- [25] R. EVERSON AND L. SIROVICH, *The Karhunen-Loeve Procedure for Gappy Data*, Journal of the Optical Society of America, 12 (1995), pp. 1657–1664.
- [26] F. GHAVAMIAN, P. TISO, AND A. SIMONE, *POD-DEIM model order reduction for strain-softening viscoplasticity*, Computer Methods in Applied Mechanics and Engineering, 317 (2017), pp. 458–479.
- [27] M. A. GREPL, Y. MADAY, N. C. NGUYEN, AND A. T. PATERA, *Efficient reduced-basis treatment of nonaffine and nonlinear partial differential equations*, ESAIM: Mathematical Modelling and Numerical Analysis, 41 (2007), pp. 575–605.
- [28] T. HASTIE, R. TIBSHIRANI, AND J. FRIEDMAN, *The Elements of Statistical Learning*, Springer, 2009.
- [29] R. A. HORN AND C. R. JOHNSON, *Matrix Analysis*, Cambridge University Press, New York, NY, USA, 2nd ed., 2012.
- [30] I. C. F. IPSEN AND B. NADLER, *Refined perturbation bounds for eigenvalues of Hermitian and Non-Hermitian matrices*, SIAM Journal on Matrix Analysis and Applications, 31 (2009), pp. 40–53.
- [31] Y. MADAY AND O. MULA, *A generalized empirical interpolation method: Application of reduced basis techniques to data assimilation*, in Analysis and Numerics of Partial Differential Equations, F. Brezzi, P. Colli Franzone, U. Gianazza, and G. Gilardi, eds., Springer, 2013, pp. 221–235.
- [32] Y. MADAY, O. MULA, A. PATERA, AND M. YANO, *The generalized empirical interpolation method: Stability theory on Hilbert spaces with an application to the Stokes equation*, Computer Methods in Applied Mechanics and Engineering, 287 (2015), pp. 310–334.
- [33] K. MANOHAR, B. W. BRUNTON, J. N. KUTZ, AND S. L. BRUNTON, *Data-Driven Sparse Sensor Placement for Reconstruction*, ArXiv e-prints, (2017).

- [34] K. MANOHAR, S. L. BRUNTON, AND J. N. KUTZ, *Environment identification in flight using sparse approximation of wing strain*, Journal of Fluids and Structures, 70 (2017), pp. 162 – 180.
- [35] G. MIGLIORATI, F. NOBILE, AND R. TEMPONE, *Convergence estimates in probability and in expectation for discrete least squares with noisy evaluations at random points*, Journal of Multivariate Analysis, 142 (2015), pp. 167 – 182.
- [36] P. MLINARIĆ, S. GRUNDEL, AND P. BENNER, *Efficient model order reduction for multi-agent systems using qr decomposition-based clustering*, in Decision and Control (CDC), 2015 IEEE 54th Annual Conference on, IEEE, 2015, pp. 4794–4799.
- [37] B. PEHERSTORFER, D. BUTNARU, K. WILLCOX, AND H. BUNGARTZ, *Localized discrete empirical interpolation method*, SIAM Journal on Scientific Computing, 36 (2014), pp. A168–A192.
- [38] B. PEHERSTORFER AND K. WILLCOX, *Online adaptive model reduction for nonlinear systems via low-rank updates*, SIAM Journal on Scientific Computing, 37 (2015), pp. A2123–A2150.
- [39] B. PEHERSTORFER, K. WILLCOX, AND M. GUNZBURGER, *Survey of multifidelity methods in uncertainty propagation, inference, and optimization*, SIAM Review, 60 (2018), pp. 550–591.
- [40] S. B. POPE, *Simple models of turbulent flows*, Physics of Fluids, 23 (2011), p. 011301.
- [41] S. SARGSYAN, S. L. BRUNTON, AND J. N. KUTZ, *Nonlinear model reduction for dynamical systems using sparse sensor locations from learned libraries*, Phys. Rev. E, 92 (2015), p. 033304.
- [42] B. SCHÖLKOPF, A. SMOLA, AND K.-R. MÜLLER, *Nonlinear component analysis as a kernel eigenvalue problem*, Neural computation, 10 (1998), pp. 1299–1319.
- [43] P. SESHADRI, A. NARAYAN, AND S. MAHADEVAN, *Effectively subsampled quadratures for least squares polynomial approximations*, SIAM/ASA Journal on Uncertainty Quantification, 5 (2017), pp. 1003–1023.
- [44] H. WEYL, *Das asymptotische verteilungsgesetz der eigenwerte linearer partieller differentialgleichungen (mit einer anwendung auf die theorie der hohlraumstrahlung)*, Mathematische Annalen, 71 (1912), pp. 441–479.
- [45] J. H. WILKINSON, *The Algebraic Eigenvalue Problem*, Oxford University Press, 1988.
- [46] K. WILLCOX, *Unsteady flow sensing and estimation via the gappy proper orthogonal decomposition*, Computers & Fluids, 35 (2006), pp. 208 – 226.
- [47] H. ZHA, X. HE, C. DING, M. GU, AND H. D. SIMON, *Spectral relaxation for k-means clustering*, in Advances in Neural Information Processing Systems 14, T. G. Dietterich, S. Becker, and Z. Ghahramani, eds., MIT Press, 2002, pp. 1057–1064.
- [48] Y. B. ZHOU, *Model reduction for nonlinear dynamical systems with parametric uncertainties*, PhD thesis, Massachusetts Institute of Technology, 2012.
- [49] R. ZIMMERMANN, B. PEHERSTORFER, AND K. WILLCOX, *Geometric subspace updates with applications to online adaptive nonlinear model reduction*, SIAM Journal on Matrix Analysis and Applications, 39 (2018), pp. 234–261.
- [50] R. ZIMMERMANN AND K. WILLCOX, *An accelerated greedy missing point estimation procedure*, SIAM Journal on Scientific Computing, 38 (2016), pp. A2827–A2850.